

Atomic force microscopy-based mechanobiology

Michael Krieg¹, Gotthold Fläschner², David Alsteens³, Benjamin M. Gaub², Wouter H. Roos⁴, Gijs J. L. Wuite⁵, Hermann E. Gaub⁶, Christoph Gerber⁷, Yves F. Dufrêne³ and Daniel J. Müller^{2*}

Abstract | Mechanobiology emerges at the crossroads of medicine, biology, biophysics and engineering and describes how the responses of proteins, cells, tissues and organs to mechanical cues contribute to development, differentiation, physiology and disease. The grand challenge in mechanobiology is to quantify how biological systems sense, transduce, respond and apply mechanical signals. Over the past three decades, atomic force microscopy (AFM) has emerged as a key platform enabling the simultaneous morphological and mechanical characterization of living biological systems. In this Review, we survey the basic principles, advantages and limitations of the most common AFM modalities used to map the dynamic mechanical properties of complex biological samples to their morphology. We discuss how mechanical properties can be directly linked to function, which has remained a poorly addressed issue. We outline the potential of combining AFM with complementary techniques, including optical microscopy and spectroscopy of mechanosensitive fluorescent constructs, super-resolution microscopy, the patch clamp technique and the use of microstructured and fluidic devices to characterize the 3D distribution of mechanical responses within biological systems and to track their morphology and functional state.

Mechanobiology focuses on how physical forces and the mechanical properties of proteins, protein assemblies, cells and tissues contribute to signalling, development, cell division, differentiation and sorting, physiology and disease^{1–4}. On virtually any scale, ranging from organisms^{2,4} to components such as organs^{5,6}, tissues^{3,7}, cells^{8–10}, viruses^{11,12}, complex extracellular or intracellular architecture (including vesicles, the extracellular matrix or actin network^{13,14}) or single proteins^{15–17}, biological systems respond to mechanical forces and generate mechanical cues.

In mechanobiology, living systems are described by cycles of mechanosensation, mechanotransduction and mechanoreponse^{2,18}. In addition to its state, the functional response of a living system depends on the nature of the mechanical signal, whether it is applied at the nanometre or micrometre scale, for a short or long time, with low or high magnitude, and on whether it is scalar or vectorial. Nanotechnological and microtechnological approaches have enabled tremendous progress in quantifying the mechanical properties of biological systems. The links between mechanical response, morphology and function, however, are conspicuously ill understood.

The most widely used approaches to structurally map the mechanical properties and responses of biological systems, ranging from millimetre to sub-nanometre

resolution and from micronewton to piconewton sensitivity, are based on atomic force microscopy (AFM)^{19,20}. In this Review, we survey the exciting developments in AFM-based approaches towards the morphological mapping of a wide variety of mechanical properties and the characterization of the functional response of biological systems under physiologically relevant conditions. We further discuss key challenges and caveats that have to be taken into account to overcome the limitations of AFM-based approaches to more fully describe the mechanical properties of living systems and highlight how complementary techniques can contribute to directly linking the functional responses of complex biological systems to mechanical cues.

Characterizing biosystems by AFM

The introduction of AFM in 1986 opened the door to imaging and manipulating matter at the atomic, molecular and cellular scales and was central to the nascent nanotechnological revolution^{21,22}. Of particular importance for the characterization of biological systems, atomic force microscopes can operate in aqueous environments and at physiological temperatures. In an atomic force microscope, a cantilever that is several micrometres long and has a molecularly sharp probe at the end is used to trace the sample topography, detecting

*e-mail: daniel.mueller@bsse.ethz.ch
<https://doi.org/10.1038/s42254-018-0001-7>

Key points

- The versatile functions of biological systems ranging from molecules, cells and cellular systems to living organisms are governed by their mechanical properties and ability to sense mechanical cues and respond to them.
- Atomic force microscopy (AFM)-based approaches provide multifunctional nanotools to measure a wide variety of mechanical properties of living systems and to apply to them well-defined mechanical cues.
- AFM allows us to apply and measure forces from the piconewton to the micronewton range on spatially defined areas with sizes ranging from the sub-nanometre to several tens of micrometres.
- Mechanical parameters characterized by AFM include force, pressure, tension, adhesion, friction, elasticity, viscosity and energy dissipation.
- The mechanical parameters of complex biological systems can be structurally mapped, with a spatial resolution ranging from millimetres to sub-nanometres and at kinetic ranges from hours to milliseconds.
- AFM can be combined with various complementary methods to characterize a multitude of mechanical, functional and morphological properties and responses of complex biological systems.

the forces between the probe and sample with piconewton sensitivity. AFM topographs have an exceptionally high signal-to-noise ratio, which enables, for example, the direct observation of single proteins in cellular membranes at sub-nanometre resolution without the need for chemical fixation or labelling²⁰. It was quickly recognized that the atomic force microscope probe can be used as a nanotool to characterize and design the surfaces of biological systems¹⁹. The simplicity of the principle of operation of AFM allows users to swiftly adjust this technique to address the mechanobiological property of interest (FIG. 1). However, although imaging and mechanical sensing by AFM might appear straightforward, several intricacies complicate the acquisition of quantitative data (FIG. 2). This section thus focuses on the key points that need to be taken into account to reach this goal.

Probing mechanical properties. The easiest way to measure mechanical properties by AFM is to indent the probe into the sample and to record the applied force, which is proportional to the cantilever deflection, and the distance travelled by the probe in a force–distance (FD) curve (FIG. 2a,b). Recorded upon approaching and retracting the probe, FD curves measure the mechanical deformation and response of the sample under load. Force can also be plotted against time in force–time (FT) curves, which are particularly useful if the force

applied by the indenting probe or the indentation depth of the probe is to be held constant^{23,24} (FIG. 2c,d). These mechanical readouts are particularly useful when the sample changes mechanical properties with time^{25,26} or viscoelastic properties need to be determined^{27–29}. To extract the Young's modulus from the apparent stiffness measured by AFM (BOX 1; TABLE 1), it is necessary to calculate the mechanical stress applied, which is the force per contact area of the probe and sample (measured in N m^{-2} or Pa). However, the deeper a probe indents the sample, the more difficult it is to estimate how it interacts with and deforms the biological sample. Such estimations, which become notoriously difficult when using common pyramidal atomic force microscope probes, may be simplified by using cylindrical or spherical probes^{30–32} (FIG. 2e). Indenting a sharp probe into a complex biological system enables the measurement of the mechanical properties only locally. The description of heterogeneous sample properties thus requires either multiple spatially discrete measurements or the use of larger probes to integrate properties over larger areas. For example, micrometre-sized spheres can be attached to an atomic force microscope cantilever³³. Alternatively, the mechanical properties of entire cells^{31,34} can be characterized by confining single cells between the parallel plates of a support and a wedged cantilever^{25,35}.

To address the heterogeneity of biological systems, various AFM imaging modes have been introduced to map mechanical properties to morphology^{19,20,36}. The most common approach records at least one FD curve for every pixel of the AFM topography (FIG. 2g). FD-based AFM can record several hundreds of thousands of force curves per topography, which makes the data analysis labour-intensive and calls for automated procedures³⁷. If the experiment has been conducted properly and a suitable model has been chosen for data analysis (as explained below), the atomic force microscope user obtains topographs and multiparametric maps describing the mechanical properties of the sample^{20,37}.

Establishing physiologically relevant conditions. AFM can be carried out under the physiological conditions required to maintain the native functional and morphological state of a biological system. Such conditions mostly include full immersion of the sample in a buffer solution, an adjustable temperature and atmospheric control (FIG. 1f). Atomic force microscope users should be cautious of drying or chemically fixing their biological samples, as these procedures can lead to severe morphological, mechanical and functional artefacts^{38–40}. Other common pitfalls are inappropriate choice of buffer solution or experimenting on mammalian cells at room temperature, at which they hardly respond to mechanical cues in a native-like manner. For instance, mammalian cells deprived of buffer solutions and lacking nutrients or survival factors can quickly change their physiological properties and even undergo apoptosis⁴¹. Furthermore, many primary cell types, such as isolated cancer cells or neurons and induced pluripotent stem cells, require stringent media formulation and osmolarity. Establishing the appropriate physiological conditions

Author addresses

¹Neurophotonics and Mechanical Systems Biology, Institute of Photonic Sciences (ICFO), Barcelona, Spain.

²Department of Biosystems Science and Engineering, Eidgenössische Technische Hochschule (ETH) Zürich, Basel, Switzerland.

³Louvain Institute of Biomolecular Science and Technology, Université catholique de Louvain, Louvain-la-Neuve, Belgium.

⁴Moleculaire Biofysica, Zernike Instituut, Rijksuniversiteit Groningen, Groningen, Netherlands.

⁵Department of Physics and Astronomy, Vrije Universiteit Amsterdam, Amsterdam, Netherlands.

⁶Applied Physics, Ludwig-Maximilians Universität (LMU) Munich, Munich, Germany.

⁷Swiss Nanoscience Institute (SNI), Institute of Physics, University of Basel, Basel, Switzerland.

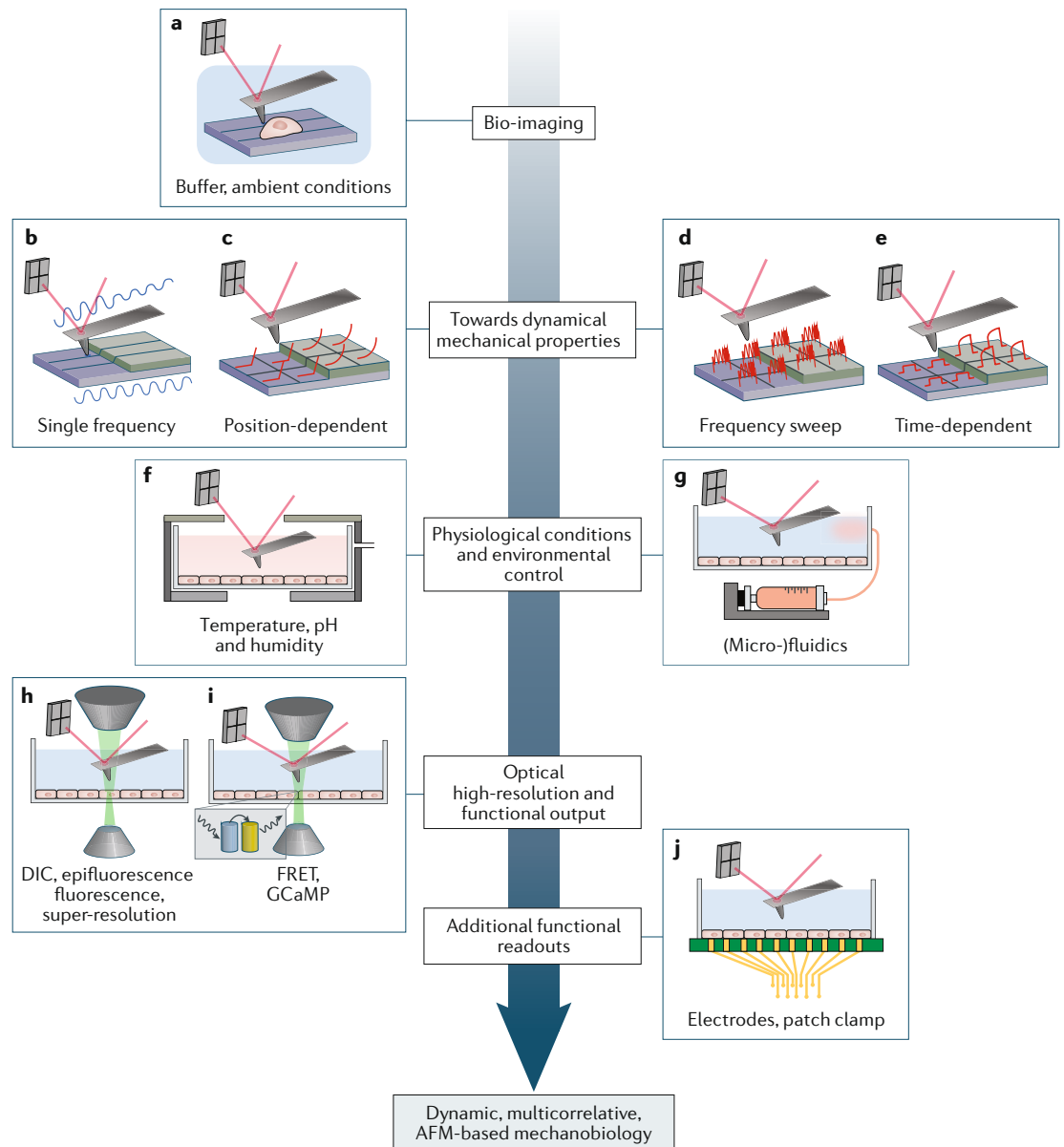


Fig. 1 | Key operation modes of atomic force microscopy to quantitatively map the mechanical properties of biological systems. **a** | Bio-imaging: the optical detection of cantilever deflection enables measurement of the surface of a biological system in an aqueous solution. The cantilever geometry and material can be selected to suit the application, and the pyramidal-shaped stylus attached to the cantilever can be replaced with various probes of different sizes and shapes to sense different sample properties. **b** | Force modulation: scanning the probe across the surface while applying a driving signal makes the cantilever oscillate. The alternating current component of the cantilever deflection signal provides information on the mechanical properties of the sample. **c** | Force mapping: a biological system is imaged, while its mechanical properties are simultaneously mapped pixel-by-pixel using spectroscopy based on force-distance and/or force-time curves. **d** | It is also possible to acquire pixel-by-pixel measurements of the mechanical response of the system to an atomic force microscope probe modulated at varying frequencies. **e** | Alternatively, it is possible to acquire its time-dependent mechanical response to an indenting atomic force microscope probe. **f** | Customized atomic force microscope chambers allow the mechanical characterization and simultaneous observation (by light microscopy) of cellular systems under incubator conditions, including controlled pH, CO₂ concentration, humidity, temperature and composition of the buffer solution. **g** | Chemical or biological compounds can be exchanged to systematically screen mechanobiological phenomena. **h** | Optical microscopy, spectroscopy and atomic force microscopy (AFM) can be combined for the morphological and mechanical characterization of complex biological systems. **i** | The optical readout of mechanical properties and biological functions using fluorescence sensors can be combined with AFM-based characterization and manipulation. **j** | Simultaneous physiological and mechanobiological characterization can be obtained by introducing complementary tools, including the patch clamp technique or multielectrode arrays. Most of these modalities (panels **a–j**) cross-fertilize each other, ultimately leading to combinatorial AFM. DIC, differential interference contrast; FRET, Förster resonance energy transfer; GCaMP, genetically encoded calcium indicator consisting of green fluorescent protein, calmodulin and M13 protein.

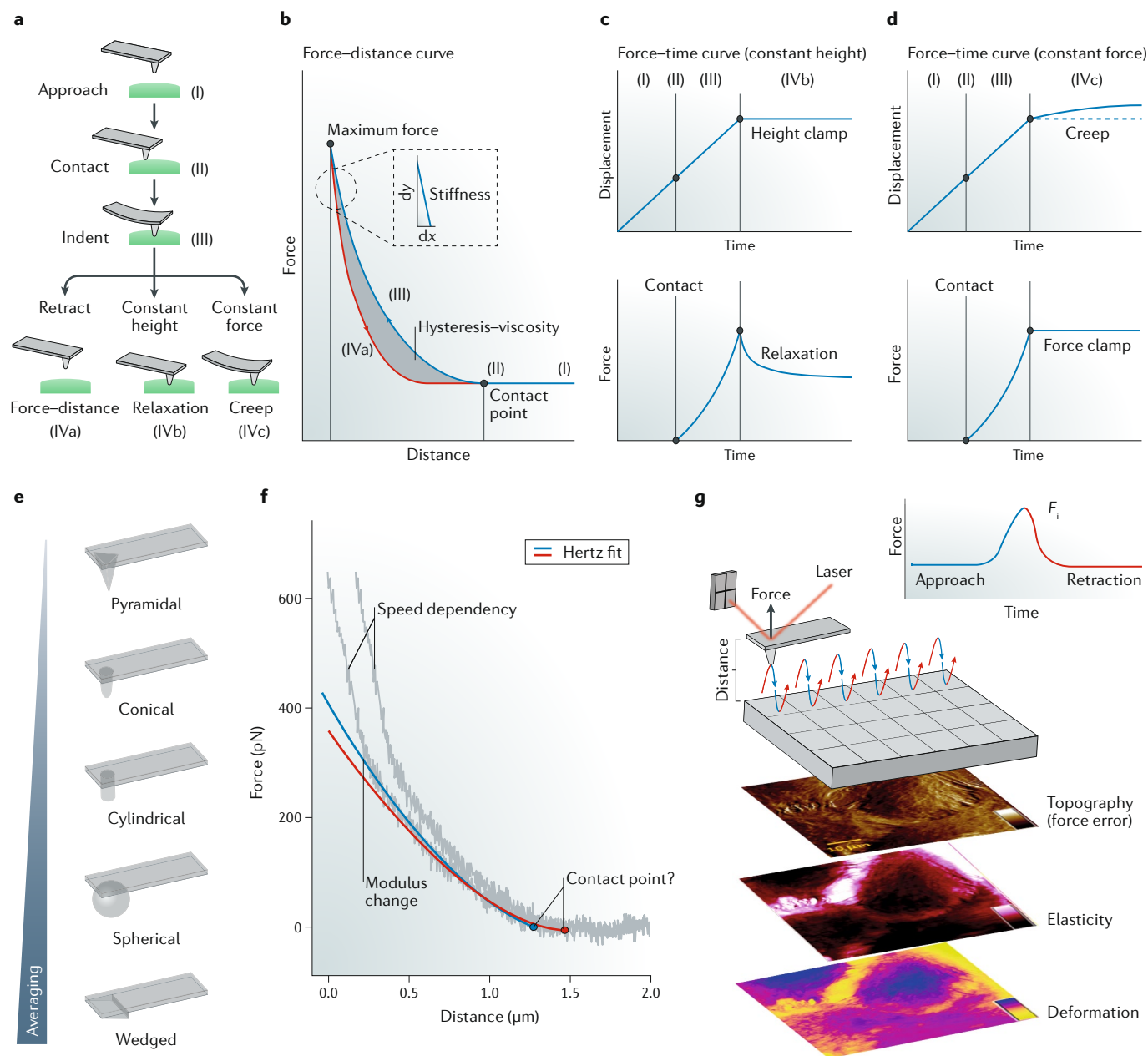


Fig. 2 | Probing, quantifying and mapping the mechanical properties of biological systems. **a** | Schematic illustration of the methods used for quantifying the mechanical responses of a biological system to the indentation of an atomic force microscope probe. **b** | Example of force–distance (FD) curve: the probe indents the sample until a defined force is reached (blue approach curve) and the cantilever is retracted (red retraction curve). From the approach FD curve, the contact point between the probe and sample and the sample stiffness can be estimated. From the difference between the approach and retraction curves, the sample viscosity can be estimated. **c** | Example of time-dependent indentation curve (constant height): the probe indents the sample and is then kept at a constant height. The force recorded by the cantilever quantifies the mechanical response of the sample. **d** | Example of time-dependent indentation curve (constant force): the probe indents (or confines) the sample, and the cantilever is kept at a constant deflection (force). The displacement of the cantilever quantifies the mechanical response of the sample. **e** | Different probes can be used for the mechanical characterization of biological systems. The larger the probe contacting the sample, the more the measurement will average out over a larger sample area. **f** | Typical challenges encountered when analysing FD (or force–time (FT)) curves are defining the contact point, fitting the slope of the approach curve (different fits lead to different elastic moduli) and addressing changes in the apparent elastic modulus due to sample heterogeneity or inadequate data acquisition. A speed-dependent behaviour indicates that the sample is viscoelastic. In this example, the grey curves are data acquired at different speeds. Blue and red curves are fits based on the Hertz model, which assume different contact points for the left-most grey curve. **g** | FD-based atomic force microscopy can be used to contour the sample topography while measuring the elastic and inelastic deformation, viscoelasticity, energy dissipation, mechanical work, pressure and tension. For each pixel of the topography, at least one FD curve is recorded. F_i , indentation force. Panel **g** is adapted with permission from REF.¹⁴⁵, Elsevier.

Box 1 | Contact models

The apparent stiffness of a sample, as measured by a force–distance curve, is defined as $k_{\text{app}} = dF/d\delta$, where F is the force exerted on the sample by the indenting atomic force microscope probe and δ is the resulting sample deformation. k_{app} depends on the contact area between the probe and sample, which generally changes with the indentation depth and speed, probe geometry and sample properties, including the roughness, viscoelastic response and adhesion. To extract the experiment-independent Young's modulus, elastic continuum theories are employed to describe the sample deformation. The basic models, which are the Hertz⁴⁸, Johnson–Kendall–Roberts (JKR)⁵⁰ and Derjaguin–Müller–Toporov (DMT)¹⁷² models, assume that the sample is purely elastic, shows no substructure and expands infinitely. In practice, these general assumptions mean that the applied strains should not exceed 20%, and probes should be blunt and indent less than 10% of the sample thickness, as summarized in the table below, together with other practical consequences of these assumptions. Whereas the Hertz model does not take into account surface forces (such as adhesion), the two other models do, though in different ways. Originally introduced for spherical probes contacting a flat surface, each model can be extended to other probe geometries to describe, for example, a conical stylus indenting a flat surface (Sneddon model)⁴⁹ or a sphere contacting a narrow cylinder to measure the mechanical properties of axons^{76,97}. TABLE 1 summarizes the models, the assumptions they are based on and their implications for experiments. An overview of specialized contact geometries is given in REF.¹⁷³.

Among the non-Hertzian contact models are the cortical shell liquid core (CSLC)^{144,174}, standard linear solid (SLS)⁹², poroelastic²³ and thin-shell^{11,125} models. The CSLC model describes the cell as a uniform, spherical liquid core surrounded by a distinct elastic shell. An indenting colloidal probe deforms the spherical cell shape¹⁷³, and complete shape recovery upon releasing the probe indicates a liquid-like response of the cell core. The force driving this recovery is attributed to the potential energy stored in the contractile actomyosin cortex, termed cortical tension. The timescale for cell shape recovery is determined by the viscosity of the cytoplasm. Several assumptions go into the CSLC model^{144,174}, which is a special case of the more general Maxwell model and represents a system as a spring connected in parallel with a spring and a dashpot to describe viscoelastic phenomena such as creep and stress relaxation. Complementary models, such as the SLS model^{62,175}, incorporate time-dependent effects to analyse force–distance curves, and extended Hertz models can fit force–time curves to extract time-varying elastic properties¹⁷⁶. The poroelastic model describes the dynamic response of the cellular cytoplasm or systems to mechanical indentation²³. Whereas viscoelastic materials are considered homogeneous, poroelastic materials are biphasic and composed of a viscous cytoplasm and an elastic drained cytoskeleton meshwork, and they can show strain-dependent moduli and time constants. The thin-shell model is often used to describe the purely elastic deformation of protein shells of viruses and is valid if the shell thickness is much smaller than the shell radius.

Purely elastic sample	Infinitely extended sample	Normal loading (perpendicular to sample surface)
<ul style="list-style-type: none"> • Can apply maximum strains of 20% • Need to use blunted tips • Speed-dependent Young's modulus used for viscoelastic samples 	<ul style="list-style-type: none"> • Indentation needs to be <10% of the sample thickness • Indentation area needs to be small compared with the sample dimensions 	<ul style="list-style-type: none"> • Requires correcting for the tilt of the cantilever • Artefacts appear because of the topography¹⁷⁷

(such as the buffer solution, temperature, humidity and CO₂ concentration) is therefore crucial to characterize the native functional and mechanical properties of a sample.

Choosing the atomic force microscope cantilever and probe. To correctly measure the mechanical properties of a biological system, it is critical to choose cantilevers that have spring constants similar to that of the system. If the cantilever is much stiffer than the sample, the deflection becomes minimal, and the measurement insensitive, whereas cantilevers that are too soft do not sufficiently deform the sample, leading to difficulties in estimating the sample stiffness (FIG. 2f). Several procedures for estimating the cantilever spring constant are available^{42–45}, including analysing the thermal noise of the cantilever or pressing the cantilever against a reference cantilever⁴². Nevertheless, instrumental and experimental variabilities lead to considerable variations (~30%) between different laboratories in determining the spring constant of the same cantilever^{44,45}. It is thus important to establish standardized procedures to determine cantilever spring constants and to check this calibration by probing reference samples or cantilevers^{42,45}. If the indentation is so deep that the probe

apex is entirely covered, or if the indentation depth is on the same scale as the roughness of the probe, it becomes notoriously difficult to estimate the sample deformation. Depending on the biological system under investigation and on the biological question, one can use atomic force microscope probes with well-defined shapes and dimensions ranging from the micrometre to the nanometre scale (FIG. 2e). By contrast, when the atomic force microscope probe makes only a slight indentation (a few nanometres), contamination with macromolecules from the sample and buffer solution can alter its interaction with the sample. One solution to this problem is to routinely check for contamination by indenting reference samples while characterizing the biological system of interest^{46,47}.

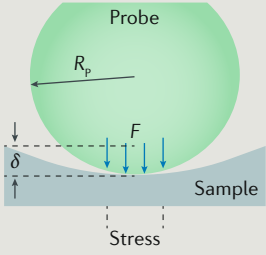
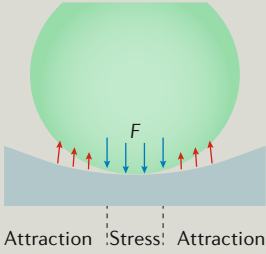
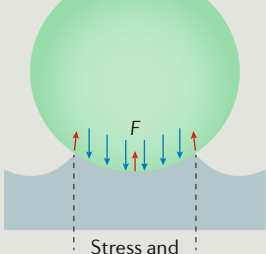
Models to extract mechanical properties. Although most commercial AFM software programs extract approximate mechanical parameters from force curves, the underlying models have several limitations. The most commonly used theoretical frameworks for approximating mechanical parameters from AFM measurements include the Hertz, Sneddon, Derjaguin–Müller–Toporov (DMT) and Johnson–Kendall–Roberts (JKR) models^{48–50}. Each model is applicable to different indenter

geometries and sample properties (BOX 1). Below, we discuss the specific limitations of these models.

To assess mechanical properties, most atomic force microscopes measure the deformation of a sample in

response to the force F applied by the indenting probe. Extracting the mechanical properties described by stress–strain curves from force curves requires a mechanical contact model, whereby the stress σ is approximated by

Table 1 | Overview of the basic continuum models and important probe geometries

Model	Probe geometry	Force	Additional assumptions	Schematic representation
Hertz	Spherical	$F = E_{\text{eff}} \cdot \left[(a^2 + R_p^2) \cdot \ln\left(\frac{R_p + a}{R_p - a}\right) - 2aR_p \right]$ $\delta = \frac{a}{2} \ln\left(\frac{R_p + a}{R_p - a}\right)$	No surface forces	
	Cylindrical	$F(\delta) = 2E_{\text{eff}} \cdot R_2 \delta$	Smooth punch profile (no edges)	–
	Conical (Sneddon model)	$F(\delta) = E_{\text{eff}} \cdot 2 \tan(\theta) / \pi \cdot \delta^2$	Infinitely sharp probe	–
	Parabolic	$F(\delta) = E_{\text{eff}} \cdot \frac{4 \cdot \sqrt{R_p}}{3} \delta^{\frac{3}{2}}$	$R_c > \delta$	–
	Blunted pyramidal	$F(\delta) = 2E_{\text{eff}} \cdot \left[\delta a - \frac{\sqrt{2}}{\pi} \frac{a^2}{\tan\theta} \left(\frac{\pi}{2} - \arcsin\frac{b}{a} \right) - \frac{a^3}{3R_p} + \sqrt{(a^2 - b^2)} \cdot \left(\frac{\sqrt{2}}{\pi} \frac{b}{\tan\theta} + \frac{a^2 - b^2}{3R_p} \right) \right]$	Cross section of pyramid modelled as a circle	–
Derjaguin–Müller–Toporov	Spherical	$F = F_{\text{Hertz}} - F_{\text{det}}$ $\delta = \frac{a}{2} \ln\left(\frac{R_p + a}{R_p - a}\right)$	<ul style="list-style-type: none"> • Long-range surface forces outside the contact area • Valid for stiff materials, small spheres and weak adhesion 	
Johnson–Kendall–Roberts	Spherical approximated with a paraboloid	$F = F_{\text{Hertz}} - 4 \sqrt{\frac{E_{\text{eff}} \cdot F_{\text{det}} a^3}{3R_p}}$ $\delta = \frac{a^2}{R_p} - 2 \sqrt{\frac{F_{\text{det}} \cdot a}{3E_{\text{eff}} R_p}}$	<ul style="list-style-type: none"> • Short-range surface forces inside the contact area • Valid for compliant materials, large spheres and strong adhesion 	
Non-Hertzian contact models				
Cortical shell liquid core	Spherical	$F = \left[2T_c \left(\frac{1}{R_c} + \frac{1}{R_p} \right) \cdot 2\pi R_p \right] \cdot \delta$	<ul style="list-style-type: none"> • Linear force–displacement curves; large membrane reservoir • Variable: T_c 	–
Standard linear solid	Conical, spherical	Analytical ¹⁷⁵ and numerical ⁹⁷ expressions	<ul style="list-style-type: none"> • Time-varying elastic modulus • Variable: viscosity 	–
Poroelastic	Spherical	$F \approx e^{-D_p \cdot t / R_p \cdot \delta}$	<ul style="list-style-type: none"> • Constant volume; timescale < 0.5 s • Variable: $D_p \approx E \xi^2 / \eta$ 	–
Thin shell	Conical	$F \approx \delta \cdot E \cdot h^2 / R_s$	<ul style="list-style-type: none"> • Point probe; $h \ll R_s$ • Variables: R_s and h 	–

δ , indentation; η , cytosolic viscosity; ν , Poisson ratio; ξ , pore size; a , contact radius; b , transition radius¹⁷⁵ of a blunt probe; D_p , poroelastic diffusion constant; E , Young's modulus; $E_{\text{eff}} = E/(1 - \nu^2)$, effective Young's modulus; F , indenting force; F_{det} , detachment force; F_{Hertz} , force in the Hertz model; h , thickness of spherical shell; θ , semi-included angle of the probe; R_c , radius of spherical cell; R_p , radius of the indenting probe; R_s , radius of spherical shell; R_2 , radius of an indenting cylinder; T_c , cortex tension.

the force per area and the deformation is approximated by the unitless strain ϵ . Conceived in 1881 to describe the non-adhesive elastic contacts between two curved surfaces (optical lenses)⁴⁸, the Hertz model is the most frequently used to obtain mechanical parameters from AFM measurements. Major assumptions underlie this model: the first is that the probe is considered a perfect sphere perpendicularly indenting a non-corrugated, plane surface. However, most atomic force microscope probes used for indentation are not perfect spheres, nor are the indented surfaces smooth on the nanoscale. Additionally, the atomic force microscope cantilever is tilted by $\sim 10^\circ$ and thus applies a non-perpendicular force during indentation. A second assumption is that the strain and elastic stress depend linearly on the Young's modulus E ($\sigma = E \cdot \epsilon$), which implies that the applied strain (the indentation) must remain small compared with the dimensions of the sample (≤ 10 – 20% of the thickness) and that the sample deformation must be fully reversible to ensure elasticity. However, complex biological structures such as living cells or tissues exhibit viscoelastic behaviour, which manifests itself as a hysteresis between the approach and retraction FD curves (FIG. 2b). Thus, the stress–strain relationship must include the viscosity η such that $\sigma = \eta \cdot d\epsilon/dt$. The viscosity of most biological systems (which stems from the friction between the constituents, such as molecules, organelles and the fibril network) can also increase with the rate at which strain is applied and thus with the indentation speed^{27–29,51}. On the other hand, viscous contributions can be reduced if measurements take place on long timescales⁵². However, there is a limit on the lowest achievable indentation speed, as biological systems can quickly remodel and respond to mechanical cues. Conversely, in transiently linked polymer networks, such as the extracellular matrix, the elasticity can become more dominating at shorter timescales^{53,54}. Another approximation of the Hertz model is that the contact area between the probe and sample is assumed to be much smaller than their dimensions. Together with the required small deformations, this criterion justifies the absence of border effects, as the stress concentrates around the area of contact and rapidly decreases within the sample. A further factor to take into account is that when a soft biological sample is indented by more than $\sim 10\%$ of its thickness, the compression of the underlying support starts contributing to the stiffness measurement⁵⁵. Thus, on a heterogeneous sample such as a cell, the measured apparent stiffness can critically depend on the location of the indentation. Additionally, it has been observed that, above certain applied strains, biological samples can stiffen and show a nonlinear mechanical response⁵⁶. Finally, the Hertz model assumes that there are no other interactions, such as adhesion or friction, between the contacting surfaces. However, adhesion is often observed when cantilevers are pressed onto cells^{57,58}. To avoid this effect, the atomic force microscope probe can be passivated with non-adhesive polyethylene glycol or other compounds⁵⁹. Alternatively, the DMT or JKR models, which include adhesive effects, can be used (BOX 1).

Even if the above conditions for applying the Hertz model are met, accurate measurements require the careful

control of experimental parameters. Extraction of the sample indentation from FD curves requires defining the point of contact (FIG. 2b,f), which can be difficult to determine. For example, as most living mammalian cells are compliant and have complex surface morphologies, a clear signature of the contact point can be missing from the FD curve, leading to an inaccuracy of a few tens of nanometres in the determination of the indentation depth. Typically, indentation depths of at least 400 nm are needed to avoid a dependence of the results on this inaccuracy⁵¹. However, for cells or tissues that are a few micrometres thick, 400 nm is critically close to the maximum indentation discussed above, while the contact area between the probe and sample becomes difficult to determine. Furthermore, the indentation of thin protein shells, such as those of viruses, is poorly described by Hertzian models; hence, thin-shell, models assuming linear deformations are more appropriate in these cases (BOX 1).

Dependence of the mechanical properties on the loading rate. The mechanical properties of biological systems depend on the loading rate (the force increasing over time) at which they are measured. Because elastic, viscous and plastic components of complex systems respond differently to mechanical cues, the mechanical properties of cells and proteinaceous assemblies change nonlinearly with the loading rate^{27,29,51,60,61} (FIG. 2f). Thus, it is meaningless to compare the mechanical properties of cells without specifying the loading rate. Varying the cantilever velocity can also enable differentiation between the possible underlying specific viscoelastic relations, such as linear or power-law rheology⁶². Additionally, complex materials respond differently to different mechanical stimuli (indentation, confinement, pressure, shear, friction, torsion, speed, or dynamic or nonlinear stimuli). Considering the anisotropic complexity of biological systems ranging from macromolecular complexes to living cells, tissues and organs, AFM experiments need to be designed carefully to apply well-defined mechanical cues and to characterize biomechanical properties over a wide range of loading rates. Another limitation is that AFM experiments mostly measure stress and strain as simple numbers, even though both are tensors describing how forces and deformation propagate in systems. The complex way forces deform structures such as macromolecules, cells or tissues is difficult to describe without complementary experimental data and assumptions or extensive theoretical simulations^{63,64}. The goal of mechanobiology must thus be to provide quantitative parameters that define how biological systems respond to force, time and spatial confinement; this objective, as outlined in the following section, can be pursued by using AFM in combination with other techniques.

Multimethodological approaches

Various cell types have been characterized by AFM to determine their Young's modulus. In many cases, however, the importance of the mechanical phenotype and its relation to physiology remained unclear. To understand how mechanical properties measured by AFM relate to cell function and morphology, AFM must be

combined with complementary techniques (FIG. 1). In addition to morphological characterization via conventional light microscopy, fluorescence microscopy can visualize tagged cellular components related to the mechanobiological measurement. For example, the dynamic assembly of fluorescently labelled actomyosin can be directly related to cell stiffening and to the cell shape changes measured by AFM^{25,26}. AFM has also been combined with confocal or light sheet fluorescence microscopy to monitor the morphological changes of a cell during indentation^{9,65,66} and with super-resolution microscopy to map the membrane properties and cytoskeletal stiffness of migrating astrocytes⁶⁷.

One of the main limitations of AFM-based mechanobiology is that the measurements are performed on the cell surface. In the past few years, fluorescence sensors have been introduced to measure the forces and pressure inside living cells^{68,69}. Other sensors measure intracellular parameters indirectly related to mechanics, such as pH, calcium concentration or membrane potential^{70,71}, or monitor the state of cellular systems or the conformation of proteins^{72–75}. Most fluorescent sensors can be either chemically attached or genetically fused to intracellular proteins, structures or compartments to specifically label them. We are just beginning to apply these sensors to correlate the mechanical properties measured by AFM to the state of the biological system and/or characterize how biological systems change state in response to mechanical cues^{9,76}. The multitude of insights revealed by such combinatorial approaches applied to the characterization of mechanobiological processes is steadily increasing. We anticipate that, in the future, these approaches will continue to be influential and will further extend the applicability of the AFM-based toolbox in mechanobiology. In the following section, we discuss some examples of such combinations.

Case studies

The basic cellular compartments and structures of mammalian cells have very different mechanical properties (FIG. 3a). To measure these properties, an atomic force microscope probe first indents the ~40–400 nm-thick soft (stiffness \approx 200–400 Pa)⁷⁷ glycocalyx surrounding the cell. Upon further indentation, the probe deforms the very soft (tension \approx 0.1–10 mN m⁻¹)⁷⁸ and thin (~5–8 nm) cell membrane — its contribution is difficult to measure because it is linked to the subjacent, 100–1,000 nm-thick and much stiffer (10–100 kPa)⁷⁹ actomyosin cortex. Moreover, while indenting through the meshwork of the cytoskeleton, the probe pushes into the viscous cytoplasm (viscosity \approx 10–100 mPa s)⁸⁰ until it encounters stiff filamentous structures (such as actin or microtubuli; stiffness \approx 0.1–1 kPa)⁸¹ and/or the nucleus (stiffness \approx 1–10 kPa)⁸². This example highlights how different cellular compartments contribute to mechanical measurements made by an indenting probe. It also shows that the mechanical anisotropy of a cell cannot be described well by contact models assuming a smooth, homogeneous and infinitely extended surface (BOX 1). It is thus necessary to extend the models to describe, for example, the poroelastic properties of the cytoplasm²³.

We examine a few case studies to highlight insights and mechanical phenotypes derived from AFM measurements that would hardly have been possible with other techniques.

Tissues, organs and organisms. Whereas AFM is regularly applied to the study of molecules and cells, relatively little work has been devoted to measuring the mechanical properties of tissues and organisms and to relate these measurements to function. It has been shown that the substrate stiffness can guide the differentiation of stem cells into various tissues^{83,84}. AFM measurements have revealed that the stiffness of differentiated cells matches that of the substrate⁸⁵, indicating that the physical nature of the environment can guide the proliferation and mechanical properties of cells. Likewise, neurons can sense and respond to the stiffness of the surrounding tissue⁸⁶. Recently, AFM-based force mapping combined with fluorescence microscopy showed that axons preferentially grow into brain regions, exposing certain stiffnesses⁸⁶. Localized injury of the neocortex leads to considerable softening of the surrounding brain tissue, which provides a signal that inhibits neuronal regeneration by limiting axon growth⁸⁷ (FIG. 3b). It has also been demonstrated by AFM that upon detecting photons, the photosensory cells in the *Drosophila* eye contract⁸⁸. Combining optical microscopy measurements with patch clamp electrophysiology enabled the investigation of the signal pathways from photon absorption to sensory processing. AFM has also been used to characterize how, similar to animal tissues, plant tissue mechanics are involved in the regulation of morphogenesis⁸⁹ and growth⁹⁰.

Changes in cell and tissue mechanics are among the hallmarks of cancer, but how tissue stiffening relates to tumour development is less clear. To understand this process, the stiffness of mammary tumour cells and surrounding tissues was mapped in situ^{91,92}, revealing that tumour tissues are far stiffer than isolated tumour cells. Such experiments highlight the potential of AFM for the investigation of disease-related mechanical phenotypes under conditions that preserve the physiological environment^{92–95}. However, despite the advances in the use of AFM to map the mechanical properties of tissue, organs and organisms, several limitations remain. The biological system needs to be accessible by AFM, which limits this approach to the investigation of surfaces. Dissection techniques may be needed to gain deeper insight into specimens^{86,87} (FIG. 3b). To guide the atomic force microscope probe to specific locations in large tissues and organs, experiments need to be combined with optical microscopy (FIG. 3). A recent effort in this direction characterized stiffness changes required for neural crest migration in heterochronic tissue grafts⁹⁶.

Neurons. Whereas mapping the mechanical properties of single neurons in living brains is difficult, isolated neurons in culture are readily accessible. Owing to the morphological and functional complexity of neurons, it has been challenging to connect neuronal mechanics to physiology. Progress has been made by combining

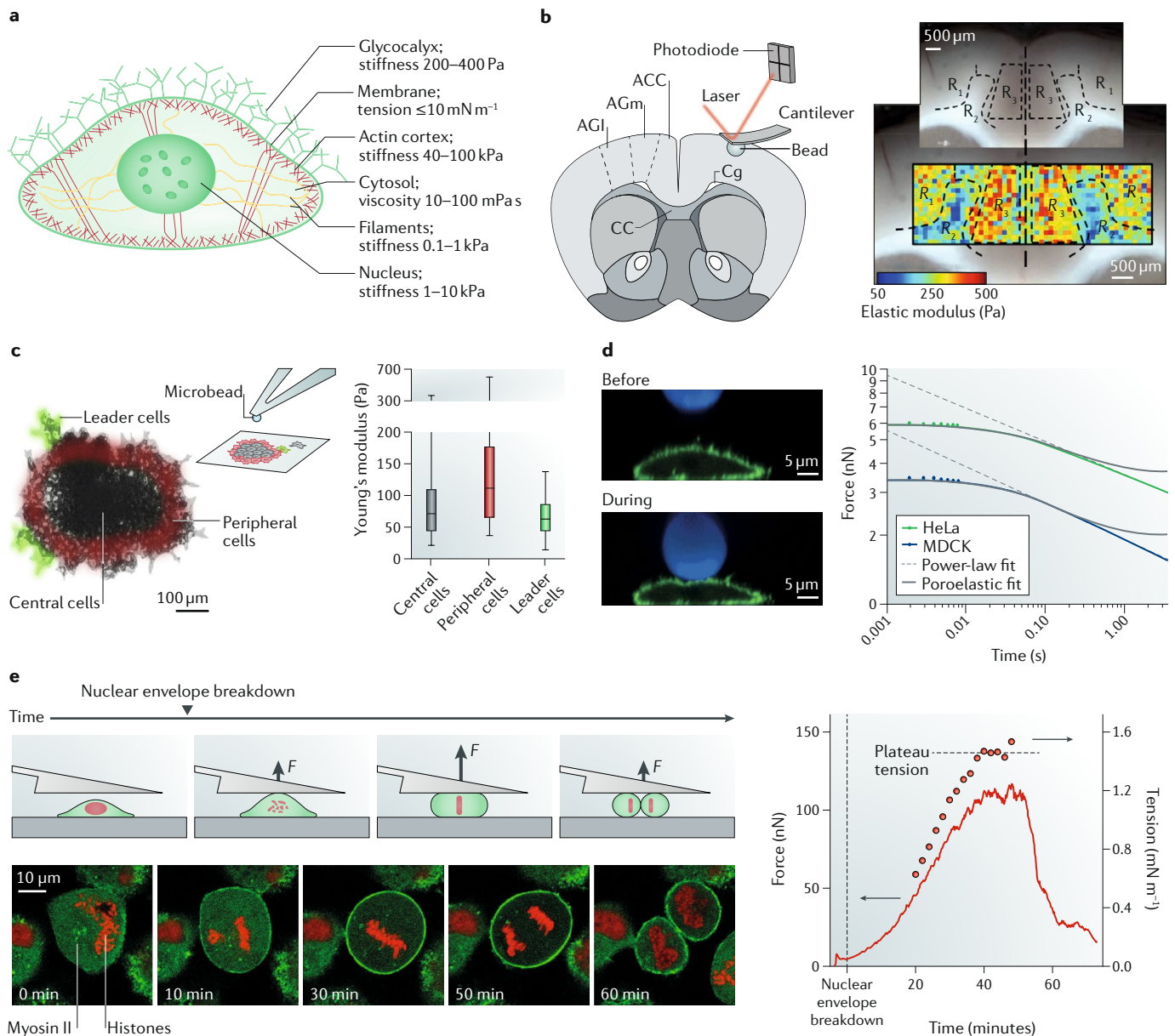


Fig. 3 | Mapping the mechanical properties of cellular systems. **a** | Schematic representation of an adherent mammalian cell with a summary of the mechanical properties of the cellular structures and compartments. **b** | Elasticity measurements of a healthy rat brain. The areas of the cortex are shown in the schematic in the left panel. CC indicates the corpus callosum, Cg denotes the cingulum, AGm represents the medial agranular, AGl indicates the lateral agranular, and ACC denotes the anterior cingulate regions of the cortex⁸⁷. A map of the elastic modulus (coloured) recorded for a healthy rat brain cortex, imaged via brightfield microscopy (greyscale), is shown in the right panel. In the coloured map, blue denotes the softest areas, and red the stiffest areas. **c** | Measurements of the elasticity of cranial neural crest cell explants. Neural crest cells undergo a transition from collective to single-cell migration during development, and the mechanisms leading to the separation of individual cells from the neural crest are still unclear. Atomic force microscopy indentation experiments (right panel) and phase-contrast microscopy (left panel) can be combined to correlate elasticity to morphological details of the explanted cellular system. The measurements show that peripheral cells are stiffer than central and semi-detached leader cells¹⁰⁶. **d** | A fluorescent micrometre-sized bead (blue) visibly indents a living HeLa cell expressing a green-fluorescent-protein-labelled membrane marker (green). For deformations on this scale, in which a large volume of cytoplasm is displaced, the experimental data presented in the right panel show that poroelasticity dominates the power-law behaviour for durations less than 0.5 s (REF.²³). Data for Madin–Darby canine kidney (MDCK) cells, which display a similar behaviour, are also shown. **e** | Probing the mechanical response of a HeLa cervical cancer cell progressing through mitosis while morphologically imaging cell shape and cell state. The cell was confined between a wedged cantilever and a support in a parallel plate assay³⁵, as shown in the top-left panel. Histones (red) and myosin II (green) were fluorescently labelled²⁹, as shown in the bottom-left panel. The time curve in the right panel shows the evolution of force and tension as the mitotic cell rounds against the confining cantilever. R, region. Panel **b** is adapted from REF.⁸⁷, CC-BY-4.0. Panel **c** is adapted with permission from REF.¹⁰⁶. Elsevier. Panel **d** is adapted from REF.²³, Springer Nature Limited. Panel **e** is adapted with permission from REF.²⁹, Elsevier.

AFM with super-resolution microscopy and in vivo Förster resonance energy transfer (FRET) tension sensors^{76,97}. It was found that the mechanical properties, function and shape of mechanosensory neurons from *Caenorhabditis elegans* depend on tension within the actin–spectrin cytoskeleton⁷⁶, whereas mutations of the tau protein homologue PTL1 increase the coupling of torque and tension in microtubule bundles, leading to neuromechanical defects during locomotion⁹⁷. AFM indentation experiments on mammalian hippocampal neurons suggest that the mechanical properties of the actin–spectrin network and its involvement in sensing mechanical cues and protecting from mechanical impact are preserved across the animal kingdom⁹⁸. Interestingly, neurons from peripheral nervous systems show higher resistance to mechanical damage than neurons from the brain⁹⁹, providing insight into how neurons may cope with mechanical trauma. Other recent advances include the use of optical microscopy to guide the atomic force microscope probe to mechanically stimulate cellular systems involved in the hearing of mice or insects and to characterize their functional response^{100–102}, leading to the observation that the response of mechanosensory neurons of the hearing organ to mechanical stimulation is nonlinear¹⁰².

Mammalian cells. AFM has been extensively used to characterize the mechanical properties of mammalian cells, making it easier to understand the contribution of the glycocalyx, cytoskeleton, cytoplasm and intracellular pressure to cell elasticity, to measure the protrusive forces of migrating cells and to assess how these mechanical properties change with cell state^{23,40,103–106} (FIG. 3c,d). Cultured cells vary in shape, and microstructured supports can be used to reduce morphological variability and to better compare the mechanical properties measured by FD-based AFM¹⁰⁷. In certain cases, such as for cells progressing through mitosis, this variability is greatly reduced this way¹⁰⁸. Confocal microscopy and AFM have revealed that mitotic mammalian cells generate intracellular pressure that the contracting actomyosin cortex directs to round the cell for division²⁵ (FIG. 3e). AFM has also been used to confine mitotic cells, which hinders the alignment of the mitotic spindle and allows the duration of mitosis to be controlled mechanically⁹. Combined with chemical perturbation and genome-wide RNA interference screens, AFM-based assays have allowed the mechanical phenotyping of genes involved in mitotic rounding and have led to the discovery of unexpected roles of disease-related genes in this fundamental cell biological process^{26,34}.

Other studies used AFM to mechanically stimulate mammalian cells and read out their real-time response using fluorescent constructs, reporting calcium flux across the membrane. Stimulation of cells expressing mechanosensitive Piezo1 ion channel proteins with a spherical indenter led to pronounced and long-lasting calcium transients¹⁰⁹. A complementary study combined patch clamp electrophysiology using a nanopipette with AFM to measure the activity of voltage-gated channels while mechanically stimulating beating cardiac cells¹¹⁰. Another method for monitoring the electrical activity of

mechanically stimulated cells is the use of planar patch clamp technology^{111,112}. Recently, oscillating atomic force microscope microcantilevers were used to measure the mass of single adherent cells with picogram sensitivity and millisecond time resolution for days while observing their morphology¹¹³. In the future, this approach might provide insight into how the mass of cells changes during growth and how mass is related to morphology and mechanical properties. Together, these results show that AFM-based mechanobiology provides new understanding, linking cellular mechanics with cellular processes and states in health and disease.

Microorganisms. Unlike mammalian cells, microbial cells are surrounded by thick, mechanically rigid cell walls, which play important roles in controlling cellular processes such as growth, division and adhesion. The advent of AFM has enabled direct, quantitative measurement of the mechanical properties of isolated wall components, such as the proteinaceous sheath¹¹⁴ and murein sacculi¹¹⁵, and of living microbial cells^{116–118}. Indentation curves on bacterial cells generally feature a nonlinear regime at lower forces followed by a linear regime at higher forces¹¹⁶. The two regimes enable the Young's modulus of the cell wall and the turgor pressure of the cell to be quantified. For example, AFM-based indentation revealed a swelling effect in *Shewanella putrefaciens* at high pH values, attributed to water exchange inside the polymeric fringe¹¹⁶. Surface appendages called fibrils were shown to strongly contribute to the softness of *Streptococcus salivarius* HB¹¹⁷. Treatment of *Staphylococcus aureus* with lysostaphin was found to decrease the bacterial spring constant and the cell wall stiffness, indicating that digestion of peptidoglycan by the enzyme leads to the formation of osmotically fragile cells¹¹⁸.

AFM has also proved useful for measuring local variations in the mechanical properties of live microorganisms. Force mapping of yeast cells revealed that the bud scar remaining after cell division is ten times stiffer than the surrounding cell wall, a finding consistent with the accumulation of chitin in this area¹¹⁹. The same method revealed major variations of mechanical properties on the diatom *Phaeodactylum tricornerutum*¹²⁰, showing that the girdle region is five times softer than the valve. Other experiments combined microfluidic devices with AFM and fluorescence microscopy to characterize how shear flow supports the formation of bacterial biofilms and affects their mechanical properties¹²¹. Furthermore, adhesion and elasticity mapped to AFM topographs of *Escherichia coli* infected with filamentous bacteriophages demonstrated that the sites of assembly and extrusion localize at the bacterial septum in the form of soft nanodomains surrounded by regions of stiff cell wall¹²² (FIG. 4a). Multiparametric AFM imaging also revealed that Zn²⁺ strongly alters the structural, mechanical and adhesive properties of the *S. aureus* surface¹²³.

Viruses. AFM measurements of viruses have revealed a surprising range of mechanical properties^{11,12,124}. The protein capsid of bacteriophage φ29, for instance, shows a Young's modulus higher than 1 GPa (REF.¹²⁵), whereas

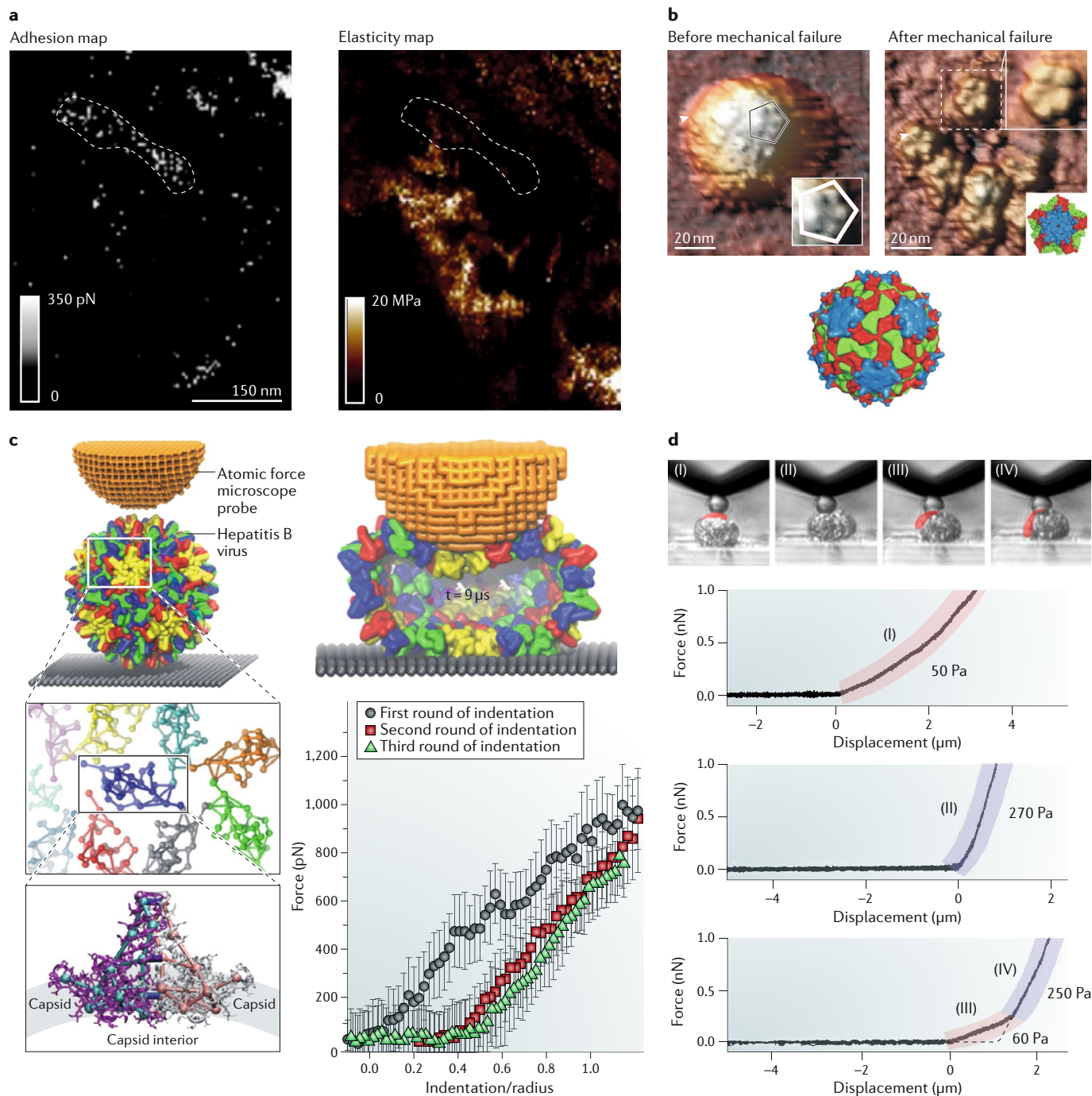
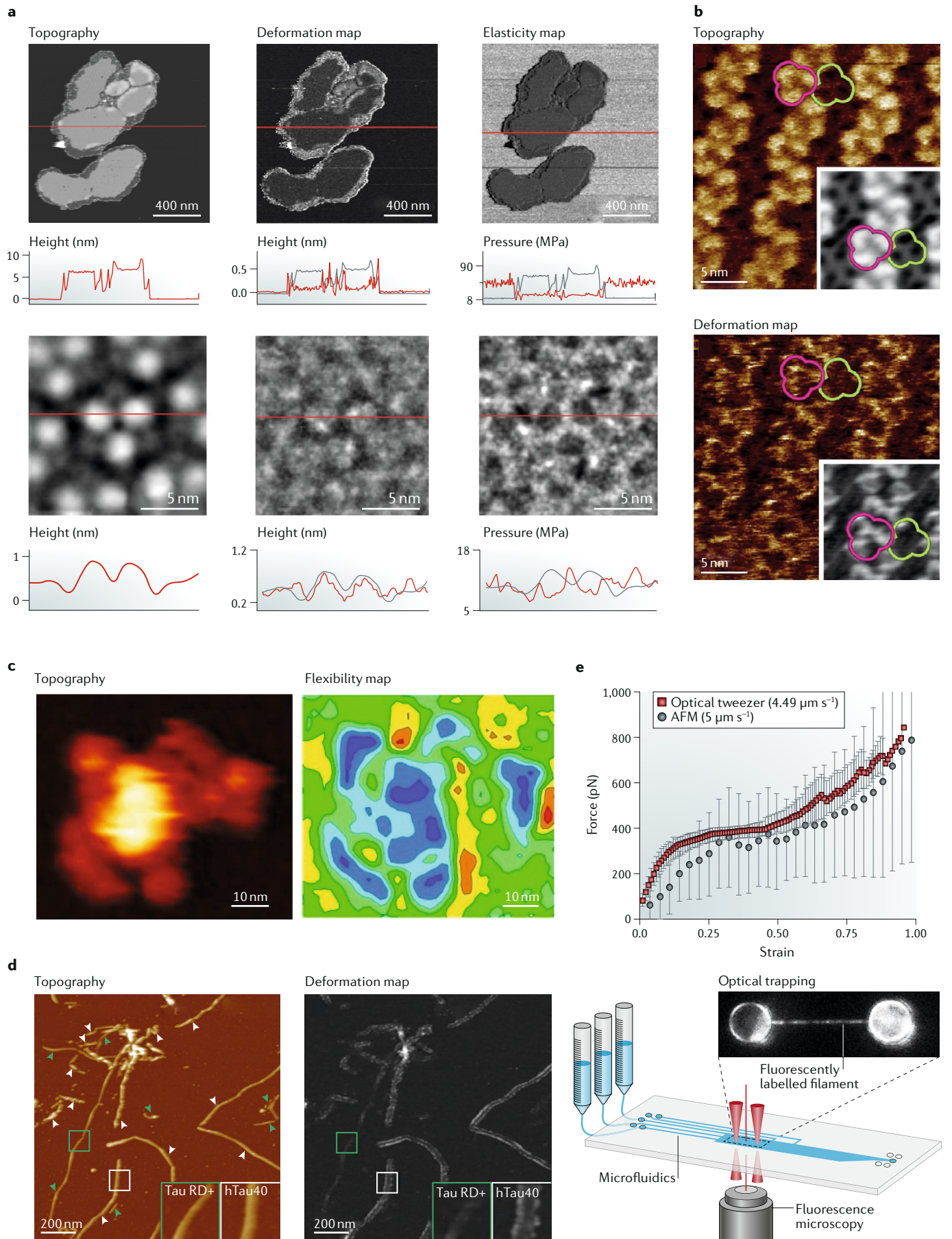


Fig. 4 | Mapping the mechanical properties of microorganisms, viruses and blebbing cell membranes. **a** | Adhesion (left panel) and elasticity (right panel) maps of the surface of an *Escherichia coli* bacterium infected by bacteriophages. Sites of bacteriophage assembly and extrusion (light-grey dots on the adhesion map) localize in soft nanodomains surrounded by a stiff cell wall (the dashed line is a guide to the eye separating the soft and the stiff areas)¹²². **b** | Surface rendering of the viral capsid of a *Triatoma* virus (bottom panel) and atomic force microscopy images acquired before and after mechanical failure due to indentation (top panels). The insets show pentamers of the intact and broken viral capsid¹³⁰. **c** | Molecular dynamics simulation of the deformation of a hepatitis B virus by an atomic force microscope probe. The images show the coarse graining of an indented shell and the conformation of the capsid at maximum indentation; the graph displays the corresponding simulated force curves, recording three subsequent rounds of indentation¹⁴³. **d** | Atomic force microscopy and side-view optical microscopy are combined to observe single cranial neural crest (CNC) cells forming membrane blebs and correlating the resulting stiffness changes. The side views of the CNC cell and beaded atomic force microscope cantilever are shown, accompanied by the corresponding force curves. I corresponds to a blebbing cell, II corresponds to a non-blebbing cell and both III and IV correspond to the case of a motile bleb moving out of the probe and cell contact area. While the stiffness of the CNC cell is ~ 270 Pa, the stiffness of a bleb is only ~ 50 – 60 Pa (REF.¹⁴⁹). Panel **a** is adapted from REF.¹²², Springer Nature Limited. Panel **b** is adapted from REF.¹³⁰, Springer Nature Limited. Panel **c** is adapted with permission from REF.¹⁴³, Elsevier. Panel **d** is adapted from REF.¹⁴⁹, CC-BY-3.0.



the capsid of the hepatitis B virus shows a Young's modulus lower than 0.5 GPa (REF.¹²⁶). This difference is thought to originate from the packaging of viral DNA into the capsid¹²⁷. The genome itself can also affect viral mechanics and has been shown to reinforce the capsid of the minute virus of mice^{128,129}. For the insect *Triatoma* virus (FIG. 4b), an intricate pH-dependent reinforcement occurs for RNA-containing capsids at neutral pH, whereas under alkaline conditions, the RNA destabilizes the capsids¹³⁰. This mechanical switch has been related to the genome delivery pathway. Obviously, the capsid architecture influences their stability, and some viruses develop an intrinsic stress to reinforce their shell. In particular, ϕ 29 and norovirus capsids are pre-stressed anisotropically and isotropically, respectively, to increase mechanical stability^{131,132}. AFM can also measure how viral stability changes with maturation, as has been shown for the HK97 phage¹³³ and HIV¹³⁴.

Recently, AFM and fluorescent microscopy provided insight into the capsid breakdown and DNA release of adenoviruses. This process was mechanically induced by the atomic force microscope probe and visualized by fluorescently staining the viral genome¹³⁵. Mechanical studies of protein shells are not limited to viruses containing the native genomic content¹³⁶. For example, experiments have been performed on cowpea chlorotic mottle virus loaded with phthalocyanine dyes¹³⁷, bacterial nanocompartment encapsulins and *Aquifex aeolicus* lumazine synthase^{138,139}, eukaryotic vaults¹⁴⁰ and artificial designer protein shells such as octahedral O3-33 cages¹³⁸. Virus–cell interactions can also be characterized by AFM, and the initial binding of

both influenza and rabies viruses to eukaryotic cells has been shown to be multivalent^{141,142}. In addition, the mechanical phage extrusion from bacteria has been scrutinized by AFM¹²². Finite-element and coarse-grain molecular dynamics simulations can provide mechanical information to complement the data and aid the interpretation of experimental results^{63,128,143} (FIG. 4c).

Cell membranes and vesicles. AFM is frequently used to measure the mechanical properties of cell membranes, including their dynamic attachment to the surrounding glycocalyx and the underlying actomyosin cortex. These properties are of particular importance to understanding cellular processes such as sensing, signalling, adhesion, sorting, migration and differentiation^{76,84,144}. Several attempts have been made to measure the mechanical properties of cell membranes by indentation^{104,108}. However, the thick and stiff glycocalyx coat, actomyosin cortex and cytoplasm (FIG. 3a) dominate the force–indentation relation recorded by AFM and mask the contribution of the very thin, soft cell membrane^{51,145}. A promising AFM-based approach to measuring the elasticity, viscosity and coupling of the cell membrane to the actomyosin cortex is to mechanically extract cell membrane tethers^{146–148}. Alternatively, the stiffness of membrane blebs formed by motile cells can be characterized¹⁴⁹ (FIG. 4d). The combination of AFM-based mechanical property mapping with chemical or genetic perturbation can provide mechanistic insight into the stabilizing role of the glycocalyx, of the anchors linking the membrane and actomyosin cortex and of the proteins that regulate the mechanical properties of the cortex^{29,105,108,145}. Complementary, so-called native membranes may be extracted from cells and imaged by FD-based AFM to map the mechanical properties of proteins and lipids^{61,150–153} (FIG. 5a).

Vesicular structures are abundant both in eukaryotic cells and extracellularly, where they contribute to cell–cell communication. The mechanics of small unilamellar vesicles consisting of different lipid mixtures have been studied by AFM^{154–156}. A model based on the Canham–Helfrich theory describes fluid lipid bilayers of deforming vesicles and accounts for the internal pressure that builds up after adsorption of the vesicle on the support⁴⁷. The membrane bending modulus can be derived by this model. This deformation behaviour, however, depends on the probe size^{32,47}. Multilamellar vesicles have also been characterized, showing that the number of bilayers can be estimated and that the vesicle stiffness scales with lamellarity¹⁵⁷.

Proteins, fibrils and nucleic acids. High-resolution imaging of native membrane proteins was achieved early in the development of AFM. Currently, AFM can image single membrane proteins in the native state at sub-nanometre resolution and observe them working with unprecedented structural detail^{20,158}. Whereas initial AFM-based approaches applied different forces to visualize the deformation of single proteins at sub-nanometre resolution¹⁵⁹, current approaches map their mechanical properties in more sophisticated ways^{19,150–152} (FIG. 5a). In particular, FD-based AFM can provide the topography and maps of elastic moduli, deformation, energy dissipation or adhesion with relative ease^{37,153}. It is possible to contour single

Fig. 5 | High-resolution imaging and mapping of the mechanical properties of isolated membranes, proteins, fibrils and nucleic acids. **a** | Atomic force microscopy (AFM) enables simultaneous investigation of the topography and the different mechanical properties of both native membranes extracted from cells and proteins within the membranes. The top panels present the topography, a deformation map and an elasticity map showing a membrane from *Halobacterium salinarium*. In the plots, red lines indicate cross sections taken on each topograph and map, while grey lines show the cross section of the topograph. The bottom panels present the high-resolution topography, a deformation map and an elasticity map showing the trimeric arrangement of the light-driven proton pump bacteriorhodopsin of the membrane. The cross sections of each topography and map are also shown¹⁵³. **b** | High-resolution topography and deformation map of densely packed outer membrane protein F (OmpF) trimers¹⁶⁰. Greyscale insets show averages of the topographs and deformation maps. Pink lines outline the OmpF trimers, exposing their extracellular surfaces, whereas green lines outline the trimers, exposing their periplasmic surfaces. **c** | Topography and flexibility map of an immunoglobulin M (IgM) antibody imaged using bimodal AFM¹⁶¹. **d** | Mapping the mechanical properties of the pathogenic human amyloid tau filaments⁴⁶. The topography and deformation map show fibrils assembled from truncated human tau (TauRD, green) and full-length human tau (hTau40, white). Only hTau40 has a fuzzy polypeptide coat, visible in the deformation map as a double rim. **e** | The mechanical properties of vimentin filaments have been mapped using optical tweezers, a microfluidic device, confocal microscopy and AFM. Using optical tweezers, the force–strain curves of individual vimentin filaments are measured and compared with the results of AFM experiments applying the same strain to the filaments¹⁶⁵. The schematic in the bottom panel shows the optical trapping setup. Panel **a** is adapted from REF.¹⁵³, Springer Nature Limited. Panel **b** is adapted with permission from Muller, D. J. Quantitative imaging of the electrostatic field and potential generated by a transmembrane protein pore at subnanometer resolution. *Nano Lett.* **13**, 5585–5593. Copyright (2013) American Chemical Society. Panel **c** adapted with permission from REF.¹⁶¹, copyrighted by the American Physical Society. Panel **d** is adapted with permission from REF.⁴⁶, PNAS. Panel **e** is adapted from REF.¹⁶⁵, CC-BY-3.0.

pore-forming membrane proteins while measuring their mechanical properties (FIG. 5b) and simultaneously probing the mechanical repulsion generated by the electrical field of the pore¹⁶⁰. Bimodal AFM imaging provides a powerful alternative to image water-soluble or membrane proteins and to map their mechanical properties^{36,161} (FIG. 5c). In many of these applications, it is useful to complement the structural and mechanical information derived by AFM with molecular dynamics simulations^{63,143}.

Amyloid fibrils are involved in various neurodegenerative diseases, and their chemical and biological properties have been investigated for decades. The soft polypeptide coat surrounding the stiffer fibrils assembled from pathological human tau was visualized for the first time by FD-based AFM⁴⁶ (FIG. 5d). It was found that the extension, stiffness and interactions of the so-called fuzzy coat depend on the pH and ion concentration of the buffer solution. The interactions can cause tau fibrils to aggregate, which is a hallmark of Alzheimer disease. Other AFM-based studies followed the polymorph assembly of amyloid fibrils from human tau or islet amyloid polypeptide and determined the conditions leading to fibril destabilization and disassembly^{162,163}. The force required to mechanically collapse microtubules¹⁶⁴, the nonlinear, rate-dependent force response of intermediate filaments¹⁶⁵ (FIG. 5e) and the mechanical properties of DNA origami¹⁶⁶ have also been measured by AFM.

Conclusions and outlook

We reviewed the key approaches and best working practices for measuring the mechanical properties of native biological systems by AFM and discussed the ability to work under physiological and cell culture conditions. The groundwork has been laid by a wealth of pioneering papers that describe the use of AFM to image and map the material properties of biological systems and to manipulate them^{19,167}. Now, AFM-based approaches can be used to characterize intermolecular and intramolecular interactions of biomolecular systems as well as their mechanical properties, including reversible and irreversible deformation, friction, energy dissipation, tension and pressure. The challenge in mechanobiology is to understand how biological systems sense, transduce and respond to mechanical cues. The functional state and response of complex biological systems are frequently addressed by combining AFM with optical microscopy. However, AFM is limited in that it applies mechanical stimuli and measures mechanical properties only from the outside of a biological system. The use of fluorescent constructs to specifically label structures in cells or tissues and to locally read out mechanical stress, tension or torsion and cellular parameters related to function has great potential^{68,69}. Likewise, optogenetics provides novel tools for using light to control

cellular systems through light-switchable membrane channels, pores, pumps or receptors and other cytosolic proteins¹⁶⁸. Complementary, mechanogenetic tools are being developed to control the activity of membrane proteins in response to externally applied mechanical cues^{109,169}. Such optical and mechanical stimulation of cellular systems is best characterized by combining electrophysiological tools (such as patch clamp techniques) or genetically encoded fluorescent activity indicators with AFM. Nanostructured or microstructured supports may also be used to mechanically confine or stimulate a biological system from one side while using an AFM from another side to sense the mechanical response that is actively or passively propagated through the system. These supports include nanopillars or micropillars, stretchable substrates and microfluidic devices. In the future, we expect to see a more rigorous implementation of such multimethodological approaches by applying mechanical constraints to a cellular system, measuring how this mechanical information is transduced through the system and characterizing its response.

We highlighted examples of the application of AFM to the characterization of the mechanobiological properties of biological systems ranging all the way from proteins, protein assemblies, cell membranes, cytoskeletons, cells and tissues to functional organs and organisms. Considerable effort has been made to study the mechanobiology of a wide range of organisms, including bacteria, yeast, plants, insects, animals and humans. These studies have elevated our understanding of how mechanical processes influence life. It is thus tempting to speculate about the methodologies that will further our understanding of these processes. New AFM-based assays must be developed or existing ones must be combined with complementary techniques to bridge length scales and timescales. Other than light microscopy, these techniques might include magnetic resonance imaging, scanning near-field optical microscopy, infrared spectroscopy or ultrasonic imaging. It is also intriguing to see the emergence of AFM combined with intracellular force and mechanical measurements¹⁷⁰ using, for example, magnetic or optical tweezers¹⁷¹. However, as outlined in this Review, the correct parametrization of AFM experiments alone can be challenging. Applying novel force spectroscopic techniques to biological systems will certainly require the development of complementary theories and mathematical models to guide the comprehensive analysis of experimental data. Ultimately, this analysis will teach us how biological systems sense, transduce and regulate responses to mechanical cues. More than ever, scientists from different disciplines need to collaborate to confront and solve the pressing questions in mechanobiology.

Published online 1 November 2018

- Hoffman, B. D., Grashoff, C. & Schwartz, M. A. Dynamic molecular processes mediate cellular mechanotransduction. *Nature* **475**, 316–323 (2011).
- Howard, J., Grill, S. W. & Bois, J. S. Turing's next steps: the mechanochemical basis of morphogenesis. *Nat. Rev. Mol. Cell Biol.* **12**, 392–398 (2011).
- Bruges, A. et al. Forces driving epithelial wound healing. *Nat. Phys.* **10**, 683–690 (2014).
- Petridou, N. I., Spiro, Z. & Heisenberg, C. P. Multiscale force sensing in development. *Nat. Cell Biol.* **19**, 581–588 (2017).
- Tyler, W. J. The mechanobiology of brain function. *Nat. Rev. Neurosci.* **13**, 867–878 (2012).
- Crest, J., Diz-Munoz, A., Chen, D. Y., Fletcher, D. A. & Bilder, D. Organ sculpting by patterned extracellular matrix stiffness. *eLife* **6**, e24958 (2017).
- Heisenberg, C. P. & Bellaiche, Y. Forces in tissue morphogenesis and patterning. *Cell* **153**, 948–962 (2013).
- Diz-Munoz, A., Fletcher, D. A. & Weiner, O. D. Use the force: membrane tension as an organizer of cell shape and motility. *Trends Cell Biol.* **23**, 47–53 (2013).
- Cattin, C. J. et al. Mechanical control of mitotic progression in single animal cells. *Proc. Natl Acad. Sci. USA* **112**, 11258–11263 (2015).

This paper shows that mechanical confinement by the atomic force microscope cantilever can be used to slow down and stop cells progressing through mitosis.

10. Roca-Cusachs, P., Conte, V. & Trepast, X. Quantifying forces in cell biology. *Nat. Cell Biol.* **19**, 742–751 (2017).
11. Roos, W. H., Bruinsma, R. & Wuite, G. J. L. Physical virology. *Nat. Phys.* **6**, 733–743 (2010).
12. Mateu, M. G. *Structure and Physics of Viruses* (Springer, Netherlands, 2013).
13. Fletcher, D. A. & Mullins, R. D. Cell mechanics and the cytoskeleton. *Nature* **463**, 485–492 (2010).
14. Bieling, P. et al. Force feedback controls motor activity and mechanical properties of self-assembling branched actin networks. *Cell* **164**, 115–127 (2016).
15. Bustamante, C., Chemla, Y. R., Forde, N. R. & Izhaky, D. Mechanical processes in biochemistry. *Annu. Rev. Biochem.* **73**, 705–748 (2004).
16. Puchner, E. M. & Gaub, H. E. Force and function: probing proteins with AFM-based force spectroscopy. *Curr. Opin. Struct. Biol.* **19**, 605–614 (2009).
17. Sauer, R. T. & Baker, T. A. AAA+ proteases: ATP-fueled machines of protein destruction. *Annu. Rev. Biochem.* **80**, 587–612 (2011).
18. Iskratsch, T., Wolfenson, H. & Sheetz, M. P. Appreciating force and shape—the rise of mechanotransduction in cell biology. *Nat. Rev. Mol. Cell Biol.* **15**, 825–833 (2014).
19. Alsteens, D. et al. Atomic force microscopy-based characterization and design of biointerfaces. *Nat. Rev. Mater.* **2**, 17008 (2017).
20. Dufrene, Y. F. et al. Imaging modes of atomic force microscopy for application in molecular and cell biology. *Nat. Nanotechnol.* **12**, 295–307 (2017).
21. Binnig, G., Quate, C. F. & Gerber, C. Atomic force microscope. *Phys. Rev. Lett.* **56**, 930–933 (1986). **This classical paper introduces the AFM technique.**
22. Gerber, C. & Lang, H. P. How the doors to the nanoworld were opened. *Nat. Nanotechnol.* **1**, 3–5 (2006).
23. Moendarbary, E. et al. The cytoplasm of living cells behaves as a poroelastic material. *Nat. Mater.* **12**, 253–261 (2013). **The authors combine AFM with advanced microscopy to explain that the sponge-like behaviour of cells relates to a viscous fluid (cytosol) flowing through a porous elastic matrix (cytoskeleton, organelles and macromolecules).**
24. Hecht, F. M. et al. Imaging viscoelastic properties of live cells by AFM: power-law rheology on the nanoscale. *Soft Matter* **11**, 4584–4591 (2015).
25. Stewart, M. P. et al. Hydrostatic pressure and the actomyosin cortex drive mitotic cell rounding. *Nature* **469**, 226–230 (2011). **This paper shows that to facilitate the drastic shape changes required for mitosis, animal cells generate hydrostatic pressure, which is balanced by a contracting actomyosin cortex.**
26. Ramanathan, S. P. et al. Cdk1-dependent mitotic enrichment of cortical myosin II promotes cell rounding against confinement. *Nat. Cell Biol.* **17**, 148–159 (2015).
27. Fabry, B. et al. Scaling the microtopology of living cells. *Phys. Rev. Lett.* **87**, 148102 (2001). **This paper represents a milestone in cellular rheology, as it introduces the notion of timescale-invariant mechanical properties and the power-law behaviour of cells.**
28. Deng, L. et al. Fast and slow dynamics of the cytoskeleton. *Nat. Mater.* **5**, 636–640 (2006).
29. Fischer-Friedrich, E. et al. Rheology of the active cell cortex in mitosis. *Biophys. J.* **111**, 589–600 (2016).
30. Sen, S., Subramanian, S. & Discher, D. E. Indentation and adhesive probing of a cell membrane with AFM: theoretical model and experiments. *Biophys. J.* **89**, 3203–3213 (2005).
31. Fischer-Friedrich, E., Hyman, A. A., Julicher, F., Muller, D. J. & Helenius, J. Quantification of surface tension and internal pressure generated by single mitotic cells. *Sci. Rep.* **4**, 6213 (2014).
32. Vorselen, D., Kooreman, E. S., Wuite, G. J. & Roos, W. H. Controlled tip wear on high roughness surfaces yields gradual broadening and rounding of cantilever tips. *Sci. Rep.* **6**, 36972 (2016).
33. Mahaffy, R. E., Shih, C. K., MacKintosh, F. C. & Kas, J. Scanning probe-based frequency-dependent microtopology of polymer gels and biological cells. *Phys. Rev. Lett.* **85**, 880–883 (2000).
34. Toyoda, Y. et al. Genome-scale single-cell mechanical phenotyping reveals disease-related genes involved in mitotic rounding. *Nat. Commun.* **8**, 1266 (2017). **This paper presents a genome-scale AFM-based screen that discovers unexpected genes that animal cells use to round for mitosis.**
35. Stewart, M. P. et al. Wedged AFM-cantilevers for parallel plate cell mechanics. *Methods* **60**, 186–194 (2013).
36. Garcia, R. & Herruzo, E. T. The emergence of multifrequency force microscopy. *Nat. Nanotechnol.* **7**, 217–226 (2012).
37. Dufrene, Y. F., Martinez-Martin, D., Medalsy, I., Alsteens, D. & Muller, D. J. Multiparametric imaging of biological systems by force-distance curve-based AFM. *Nat. Methods* **10**, 847–854 (2013).
38. Eisenberg, B. R. & Mobley, B. A. Size changes in single muscle fibers during fixation and embedding. *Tissue Cell* **7**, 383–387 (1975).
39. Dubochet, J. et al. Cryo-electron microscopy of vitrified specimens. *Q. Rev. Biophys.* **21**, 129–228 (1988).
40. Hoh, J. H. & Schoenenberger, C. A. Surface morphology and mechanical properties of MDCK monolayers by atomic force microscopy. *J. Cell Sci.* **107**, 1105–1114 (1994).
41. Meredith, J. E., Fazeli, B. & Schwartz, M. A. The extracellular-matrix as a cell-survival factor. *Mol. Biol. Cell* **4**, 953–961 (1993).
42. Sader, J. E. & White, L. Theoretical analysis of the static deflection of plates for atomic force microscope applications. *J. Appl. Phys.* **74**, 1–9 (1993).
43. Butt, H. J. & Jaschke, M. Calculation of thermal noise in atomic force microscopy. *Nanotechnology* **6**, 1–7 (1995).
44. te Riet, J. et al. Interlaboratory round robin on cantilever calibration for AFM force spectroscopy. *Ultramicroscopy* **111**, 1659–1669 (2011).
45. Schillers, H. et al. Standardized nanomechanical atomic force microscopy procedure (SNAP) for measuring soft and biological samples. *Sci. Rep.* **7**, 5117 (2017). **This paper introduces an approach to reducing the variability in extracting the elastic moduli of soft samples and reports on its validation in various laboratories to establish it as a standard method.**
46. Wegmann, S., Medalsy, I. D., Mandelkow, E. & Muller, D. J. The fuzzy coat of pathological human Tau fibrils is a two-layered polyelectrolyte brush. *Proc. Natl Acad. Sci. USA* **110**, E313–E321 (2013).
47. Vorselen, D., MacKintosh, F. C., Roos, W. H. & Wuite, G. J. Competition between bending and internal pressure governs the mechanics of fluid nanovesicles. *ACS Nano* **11**, 2628–2636 (2017).
48. Hertz, H. Über die Berührung fester elastischer Körper [German]. *Reine Angew. Math.* **92**, 156–171 (1881).
49. Sneddon, I. N. The relation between load and penetration in the axisymmetric boussinesq problem for a punch of arbitrary profile. *Int. J. Eng. Sci.* **3**, 47–57 (1965).
50. Johnson, K. L., Kendall, K. & Roberts, A. D. Surface energy and the contact of elastic solids. *Proc. R. Soc. A* **324**, 301–313 (1971).
51. Rigato, A., Miyagi, A., Scheuring, S. & Rico, F. High-frequency microtopology reveals cytoskeleton dynamics in living cells. *Nat. Phys.* **13**, 771–775 (2017).
52. Hassan, A. E. et al. Relative microelastic mapping of living cells by atomic force microscopy. *Biophys. J.* **74**, 1564–1578 (1998).
53. Morse, D. C. Viscoelasticity of tightly entangled solutions of semiflexible polymers. *Phys. Rev. E* **58**, R1237–R1240 (1998).
54. Broedersz, C. P. & MacKintosh, F. C. Modeling semiflexible polymer networks. *Rev. Mod. Phys.* **86**, 995–1036 (2014).
55. Dimitriadis, E. K., Horkay, F., Maresca, J., Kachar, B. & Chadwick, R. S. Determination of elastic moduli of thin layers of soft material using the atomic force microscope. *Biophys. J.* **82**, 2798–2810 (2002). **This paper introduces a helpful approach to reliably extract the mechanical properties of spread cells, as it remedies the insufficient treatment of their finite thickness within the Hertzian (and related) model.**
56. Storm, C., Pastore, J. J., MacKintosh, F. C., Lubensky, T. C. & Janmey, P. A. Nonlinear elasticity in biological gels. *Nature* **435**, 191–194 (2005).
57. Notbohm, J., Poon, B. & Ravichandran, G. Analysis of nonindentation of soft materials with an atomic force microscope. *J. Mater. Res.* **27**, 229–237 (2012).
58. Friedrichs, J. et al. A practical guide to quantify cell adhesion using single-cell force spectroscopy. *Methods* **60**, 169–178 (2013).
59. Hinterdorfer, P. & Dufrene, Y. F. Detection and localization of single molecular recognition events using atomic force microscopy. *Nat. Methods* **3**, 347–355 (2006).
60. Snijder, J., Ivanovska, I. L., Baclayon, M., Roos, W. H. & Wuite, G. J. Probing the impact of loading rate on the mechanical properties of viral nanoparticles. *Micron* **43**, 1343–1350 (2012).
61. Medalsy, I. D. & Muller, D. J. Nanomechanical properties of proteins and membranes depend on loading rate and electrostatic interactions. *ACS Nano* **7**, 2642–2650 (2013).
62. Efremov, Y. M., Wang, W. H., Hardy, S. D., Geahlen, R. L. & Raman, A. Measuring nanoscale viscoelastic parameters of cells directly from AFM force-displacement curves. *Sci. Rep.* **7**, 1541 (2017). **This paper introduces a powerful approach to extracting elastic and viscous parameters from FD curves.**
63. Zink, M. & Grubmüller, H. Mechanical properties of the icosahedral shell of southern bean mosaic virus: a molecular dynamics study. *Biophys. J.* **96**, 1350–1363 (2009).
64. Schoeler, C. et al. Mapping mechanical force propagation through biomolecular complexes. *Nano Lett.* **15**, 7370–7376 (2015).
65. Chaudhuri, O., Parekh, S. H., Lam, W. A. & Fletcher, D. A. Combined atomic force microscopy and side-view optical imaging for mechanical studies of cells. *Nat. Methods* **6**, 383–387 (2009).
66. Beicker, K., O'Brien, E. T. 3rd, Falvo, M. R. & Superfine, R. Vertical light sheet enhanced side-view imaging for AFM cell mechanics studies. *Sci. Rep.* **8**, 1504 (2018).
67. Curry, N., Ghezali, G., Kaminski Schierle, C. S., Rouach, N. & Kaminski, C. F. Correlative STED and atomic force microscopy on live astrocytes reveals plasticity of cytoskeletal structure and membrane physical properties during polarized migration. *Front. Cell Neurosci.* **11**, 104 (2017).
68. Freikamp, A., Cost, A. L. & Grashoff, C. The piconewton force awakens: quantifying mechanics in cells. *Trends Cell Biol.* **26**, 838–847 (2016).
69. Polacheck, W. J. & Chen, C. S. Measuring cell-generated forces: a guide to the available tools. *Nat. Methods* **13**, 415–423 (2016).
70. Zou, P. et al. Bright and fast multicoloured voltage reporters via electrochromic FRET. *Nat. Commun.* **5**, 4625 (2014).
71. Nekimken, A. L. et al. Pneumatic stimulation of *C. elegans* mechanoreceptor neurons in a microfluidic trap. *Lab. Chip* **17**, 1116–1127 (2017).
72. Sakaue-Sawano, A. et al. Visualizing spatiotemporal dynamics of multicellular cell-cycle progression. *Cell* **132**, 487–498 (2008).
73. Grashoff, C. et al. Measuring mechanical tension across vinculin reveals regulation of focal adhesion dynamics. *Nature* **466**, 263–266 (2010).
74. Guo, J., Wang, Y., Sachs, F. & Meng, F. Actin stress in cell reprogramming. *Proc. Natl Acad. Sci. USA* **111**, E5252–E5261 (2014).
75. Freikamp, A., Mellich, A., Klingner, C. & Grashoff, C. Investigating piconewton forces in cells by FRET-based molecular force microscopy. *J. Struct. Biol.* **197**, 37–42 (2017).
76. Krieg, M., Dunn, A. R. & Goodman, M. B. Mechanical control of the sense of touch by beta-spectrin. *Nat. Cell Biol.* **16**, 224–233 (2014).
77. O'Callaghan, R., Job, K. M., Dull, R. O. & Hlady, V. Stiffness and heterogeneity of the pulmonary endothelial glycocalyx measured by atomic force microscopy. *Am. J. Physiol. Lung Cell. Mol. Physiol.* **301**, L353–L360 (2011).
78. Morris, C. E. & Homann, U. Cell surface area regulation and membrane tension. *J. Membr. Biol.* **179**, 79–102 (2001).
79. Cartagena-Rivera, A. X., Logue, J. S., Waterman, C. M. & Chadwick, R. S. Actomyosin cortical mechanical properties in nonadherent cells determined by atomic force microscopy. *Biophys. J.* **110**, 2528–2539 (2016).
80. Janmey, P. A. & Weitz, D. A. Dealing with mechanics: mechanisms of force transduction in cells. *Trends Biochem. Sci.* **29**, 364–370 (2004).
81. Laurent, V. M. et al. Partitioning of cortical and deep cytoskeleton responses from transient magnetic bead twisting. *Ann. Biomed. Eng.* **31**, 1263–1278 (2003).
82. Lammerding, J. Mechanics of the nucleus. *Compr. Physiol.* **1**, 783–807 (2011).
83. Discher, D. E., Janmey, P. & Wang, Y. L. Tissue cells feel and respond to the stiffness of their substrate. *Science* **310**, 1139–1143 (2005).
84. Engler, A. J., Sen, S., Sweeney, H. L. & Discher, D. E. Matrix elasticity directs stem cell lineage specification. *Cell* **126**, 677–689 (2006).

85. Engler, A. J., Rehfeldt, F., Sen, S. & Discher, D. E. Microtissue elasticity: measurements by atomic force microscopy and its influence on cell differentiation. *Methods Cell Biol.* **83**, 521–545 (2007).
86. Koser, D. E. et al. Mechanosensing is critical for axon growth in the developing brain. *Nat. Neurosci.* **19**, 1592–1598 (2016).
87. Moenndarbar, E. et al. The soft mechanical signature of glial scars in the central nervous system. *Nat. Commun.* **8**, 14787 (2017).
88. Hardie, R. C. & Franze, K. Photomechanical responses in *Drosophila* photoreceptors. *Science* **338**, 260–263 (2012).
89. Peaucelle, A. et al. Pectin-induced changes in cell wall mechanics underlie organ initiation in *Arabidopsis*. *Curr. Biol.* **21**, 1720–1726 (2011).
90. Zhang, T., Vavylonis, D., Durachko, D. M. & Cosgrove, D. J. Nanoscale movements of cellulose microfibrils in primary cell walls. *Nat. Plants* **3**, 17056 (2017).
91. Lopez, J. I., Kang, I., You, W. K., McDonald, D. M. & Weaver, V. M. In situ force mapping of mammary gland transformation. *Integr. Biol.* **3**, 910–921 (2011).
92. Plodinec, M. et al. The nanomechanical signature of breast cancer. *Nat. Nanotechnol.* **7**, 757–765 (2012).
93. Cross, S. E., Jin, Y. S., Rao, J. & Gimzewski, J. K. Nanomechanical analysis of cells from cancer patients. *Nat. Nanotechnol.* **2**, 780–783 (2007). **This work introduces AFM for the mechanical phenotyping of cancer cells derived from patients.**
94. Iyer, S., Gaikwad, R. M., Subba-Rao, V., Woodworth, C. D. & Sokolov, I. Atomic force microscopy detects differences in the surface brush of normal and cancerous cells. *Nat. Nanotechnol.* **4**, 389–393 (2009).
95. Staunton, J. R., Doss, B. L., Lindsay, S. & Ros, R. Correlating confocal microscopy and atomic force indentation reveals metastatic cancer cells stiffer during invasion into collagen I matrices. *Sci. Rep.* **6**, 19686 (2016).
96. Barriga, E. H., Franze, K., Charras, G. & Mayor, R. Tissue stiffening coordinates morphogenesis by triggering collective cell migration in vivo. *Nature* **554**, 523–527 (2018).
97. Krieg, M. et al. Genetic defects in beta-spectrin and tau sensitize *C. elegans* axons to movement-induced damage via torque-tension coupling. *eLife* **6**, e20172 (2017).
98. Zhang, Y. et al. Modeling of the axon membrane skeleton structure and implications for its mechanical properties. *PLOS Comput. Biol.* **13**, e1005407 (2017).
99. Magdesian, M. H. et al. Atomic force microscopy reveals important differences in axonal resistance to injury. *Biophys. J.* **103**, 405–414 (2012).
100. Gueta, R., Barlam, D., Shneck, R. Z. & Rouso, I. Measurement of the mechanical properties of isolated tectorial membrane using atomic force microscopy. *Proc. Natl Acad. Sci. USA* **103**, 14790–14795 (2006).
101. Szarama, K. B., Gavara, N., Petralia, R. S., Kelley, M. W. & Chadwick, R. S. Cytoskeletal changes in actin and microtubules underlie the developing surface mechanical properties of sensory and supporting cells in the mouse cochlea. *Development* **139**, 2187–2197 (2012).
102. Windmill, J. F. C., Jackson, J. C., Pook, V. G. & Robert, D. Frequency doubling by active in vivo motility of mechanosensory neurons in the mosquito ear. *R. Soc. Open Sci.* **5**, 171082 (2018).
103. Rotsch, C., Braet, F., Wisse, E. & Radmacher, M. AFM imaging and elasticity measurements on living rat liver macrophages. *Cell Biol. Int.* **21**, 685–696 (1997).
104. Rotsch, C., Jacobson, K. & Radmacher, M. Dimensional and mechanical dynamics of active and stable edges in motile fibroblasts investigated by using atomic force microscopy. *Proc. Natl Acad. Sci. USA* **96**, 921–926 (1999).
105. Rotsch, C. & Radmacher, M. Drug-induced changes of cytoskeletal structure and mechanics in fibroblasts: an atomic force microscopy study. *Biophys. J.* **78**, 520–535 (2000).
106. Blaue, C., Kashef, J. & Franz, C. M. Cadherin-11 promotes neural crest cell spreading by reducing intracellular tension-Mapping adhesion and mechanics in neural crest explants by atomic force microscopy. *Semin. Cell Dev. Biol.* **73**, 95–106 (2018).
107. Rigato, A., Rico, F., Eghiaian, F., Piel, M. & Scheuring, S. Atomic force microscopy mechanical mapping of micropatterned cells shows adhesion geometry-dependent mechanical response on local and global scales. *ACS Nano* **9**, 5846–5856 (2015).
108. Matzke, R., Jacobson, K. & Radmacher, M. Direct, high-resolution measurement of furrow stiffening during division of adherent cells. *Nat. Cell Biol.* **3**, 607–610 (2001). **This is a pioneering AFM study mapping the dynamic stiffness changes of the cortex of adherent cells.**
109. Gaub, B. M. & Muller, D. J. Mechanical stimulation of piezo 1 receptors depends on extracellular matrix proteins and directionality of force. *Nano Lett.* **17**, 2064–2072 (2017).
110. Ossola, D. et al. Force-controlled patch clamp of beating cardiac cells. *Nano Lett.* **15**, 1743–1750 (2015).
111. Pamiir, E., George, M., Fertig, N. & Benoit, M. Planar patch-clamp force microscopy on living cells. *Ultramicroscopy* **108**, 552–557 (2008).
112. Upadhye, K. V., Candiello, J. E., Davidson, L. A. & Lin, H. Whole-cell electrical activity under direct mechanical stimulus by AFM cantilever using planar patch clamp chip approach. *Cell. Mol. Bioeng.* **4**, 270–280 (2011).
113. Martinez-Martin, D. et al. Inertial picobalance reveals fast mass fluctuations in mammalian cells. *Nature* **550**, 500–505 (2017). **This paper introduces AFM as a picobalance to measure the total mass of adherent cells at millisecond time resolution under cell culture conditions.**
114. Xu, W. et al. Modeling and measuring the elastic properties of an archaeal surface, the sheath of *Methanospirillum hungatei*, and the implication for methane production. *J. Bacteriol.* **178**, 3106–3112 (1996).
115. Yao, X., Jericho, M., Pink, D. & Beveridge, T. Thickness and elasticity of gram-negative murein sacculi measured by atomic force microscopy. *J. Bacteriol.* **181**, 6865–6875 (1999).
116. Gaboriaud, F., Baillet, S., Dague, E. & Jorand, F. Surface structure and nanomechanical properties of *Shewanella putrefaciens* bacteria at two pH values (4 and 10) determined by atomic force microscopy. *J. Bacteriol.* **187**, 3864–3868 (2005).
117. van der Mei, H. C. et al. Direct probing by atomic force microscopy of the cell surface softness of a fibrillated and nonfibrillated oral streptococcal strain. *Biophys. J.* **78**, 2668–2674 (2000).
118. Francius, G., Domenech, O., Mingeot-Leclercq, M. P. & Dufrene, Y. F. Direct observation of *Staphylococcus aureus* cell wall digestion by lysostaphin. *J. Bacteriol.* **190**, 7904–7909 (2008).
119. Touhami, A., Nysten, B. & Dufrene, Y. F. Nanoscale mapping of the elasticity of microbial cells by atomic force microscopy. *Langmuir* **19**, 4539–4543 (2003).
120. Francius, G., Tesson, B., Dague, E., Martin-Jezequel, V. & Dufrene, Y. F. Nanostructure and nanomechanics of live *Phaeodactylum tricornutum* morphotypes. *Environ. Microbiol.* **10**, 1344–1356 (2008).
121. Mosier, A. P., Kaloyeros, A. E. & Cady, N. C. A novel microfluidic device for the in situ optical and mechanical analysis of bacterial biofilms. *J. Microbiol. Methods* **91**, 198–204 (2012).
122. Alsteens, D., Trabelsi, H., Soumillion, P. & Dufrene, Y. F. Multiparametric atomic force microscopy imaging of single bacteriophages extruding from living bacteria. *Nat. Commun.* **4**, 2926 (2013).
123. Formosa-Dague, C., Speziale, P., Foster, T. J., Geoghegan, J. A. & Dufrene, Y. F. Zinc-dependent mechanical properties of *Staphylococcus aureus* biofilm-forming surface protein SasG. *Proc. Natl Acad. Sci. USA* **113**, 410–415 (2016).
124. Marchetti, M., Wuite, G. & Roos, W. H. Atomic force microscopy observation and characterization of single virions and virus-like particles by nano-indentation. *Curr. Opin. Virol.* **18**, 82–88 (2016).
125. Ivanovska, I. L. et al. Bacteriophage capsids: tough nanoshells with complex elastic properties. *Proc. Natl Acad. Sci. USA* **101**, 7600–7605 (2004).
126. Uetrecht, C. et al. High-resolution mass spectrometry of viral assemblies: molecular composition and stability of dimorphic hepatitis B virus capsids. *Proc. Natl Acad. Sci. USA* **105**, 9216–9220 (2008).
127. Smith, D. E. et al. The bacteriophage straight phi29 portal motor can package DNA against a large internal force. *Nature* **413**, 748–752 (2001).
128. Carrasco, C. et al. DNA-mediated anisotropic mechanical reinforcement of a virus. *Proc. Natl Acad. Sci. USA* **103**, 13706–13711 (2006). **This paper shows that the viral genome interacts with and mechanically reinforces the viral capsid.**
129. Castellanos, M., Carrillo, P. J. & Mateu, M. G. Quantitatively probing propensity for structural transitions in engineered virus nanoparticles by single-molecule mechanical analysis. *Nanoscale* **7**, 5654–5664 (2015).
130. Snijder, J. et al. Probing the biophysical interplay between a viral genome and its capsid. *Nat. Chem.* **5**, 502–509 (2013).
131. Carrasco, C. et al. Built-in mechanical stress in viral shells. *Biophys. J.* **100**, 1100–1108 (2011).
132. Baclayon, M. et al. Prestress strengthens the shell of Norwalk virus nanoparticles. *Nano Lett.* **11**, 4865–4869 (2011). **This work describes the contribution of viral domains to the mechanical stability of a viral capsid.**
133. Roos, W. H. et al. Mechanics of bacteriophage maturation. *Proc. Natl Acad. Sci. USA* **109**, 2342–2347 (2012).
134. Kol, N. et al. A stiffness switch in human immunodeficiency virus. *Biophys. J.* **92**, 1777–1783 (2007). **This work establishes a direct link between the mechanical properties of HIV and its infectivity.**
135. Ortega-Esteban, A. et al. Fluorescence tracking of genome release during mechanical unpacking of single viruses. *ACS Nano* **9**, 10571–10579 (2015).
136. Martinez-Martin, D. et al. Resolving structure and mechanical properties at the nanoscale of viruses with frequency modulation atomic force microscopy. *PLOS ONE* **7**, e30204 (2012).
137. Luque, D. Self-assembly and characterization of small and monodisperse dye nanospheres in a protein cage. *Chem. Sci.* **5**, 575–581 (2014).
138. Heinze, K. et al. Protein nanocontainers from nonviral origin: testing the mechanics of artificial and natural protein cages by AFM. *J. Phys. Chem. B* **120**, 5945–5952 (2016).
139. Snijder, J. et al. Assembly and mechanical properties of the cargo-free and cargo-loaded bacterial nanocompartment encapsulin. *Biomacromolecules* **17**, 2522–2529 (2016).
140. Llauro, A. et al. Decrease in pH destabilizes individual vault nanocages by weakening the inter-protein lateral interaction. *Sci. Rep.* **6**, 34143 (2016).
141. Sieben, C. et al. Influenza virus binds its host cell using multiple dynamic interactions. *Proc. Natl Acad. Sci. USA* **109**, 13626–13631 (2012).
142. Alsteens, D. et al. Nanomechanical mapping of first binding steps of a virus to animal cells. *Nat. Nanotechnol.* **12**, 177–183 (2017).
143. Arkhipov, A., Roos, W. H., Wuite, G. J. & Schulten, K. Elucidating the mechanism behind irreversible deformation of viral capsids. *Biophys. J.* **97**, 2061–2069 (2009).
144. Krieg, M. et al. Tensile forces govern germ-layer organization in zebrafish. *Nat. Cell Biol.* **10**, 429–436 (2008). **This work addresses a question in cell biology that is over 30 years old, that is, whether cell adhesion or cortex tension governs germ-layer organization in development.**
145. Heu, C., Berquand, A., Elie-Caille, C. & Nicod, L. Glyphosate-induced stiffening of HaCaT keratinocytes, a peak force tapping study on living cells. *J. Struct. Biol.* **178**, 1–7 (2012).
146. Sheetz, M. P. Cell control by membrane-cytoskeleton adhesion. *Nat. Rev. Mol. Cell Biol.* **2**, 392–396 (2001).
147. Krieg, M., Helenius, J., Heisenberg, C. P. & Muller, D. J. A bond for a lifetime: employing membrane nanotubes from living cells to determine receptor-ligand kinetics. *Angew. Chem. Int. Ed.* **47**, 9775–9777 (2008).
148. Vasquez, V., Krieg, M., Lockhead, D. & Goodman, M. B. Phospholipids that contain polyunsaturated fatty acids enhance neuronal cell mechanics and touch sensation. *Cell Rep.* **6**, 70–80 (2014).
149. Gonnermann, C. et al. Quantitating membrane bleb stiffness using AFM force spectroscopy and an optical sideview setup. *Integr. Biol.* **7**, 356–363 (2015).
150. Dong, M., Husale, S. & Sahin, O. Determination of protein structural flexibility by microsecond force spectroscopy. *Nat. Nanotechnol.* **4**, 514–517 (2009).
151. Medalsy, I., Hensen, U. & Muller, D. J. Imaging and quantifying chemical and physical properties of native proteins at molecular resolution by force-volume

- AFM. *Angew. Chem. Int. Ed.* **50**, 12103–12108 (2011).
152. Rico, F., Su, C. & Scheuring, S. Mechanical mapping of single membrane proteins at submolecular resolution. *Nano Lett.* **11**, 3983–3986 (2011).
153. Pfreundschuh, M., Martinez-Martin, D., Mulvihill, E., Wegmann, S. & Muller, D. J. Multiparametric high-resolution imaging of native proteins by force-distance curve-based AFM. *Nat. Protoc.* **9**, 1113–1130 (2014).
154. Liang, X., Mao, G. & Simon Ng, K. Y. Probing small unilamellar EggPC vesicles on mica surface by atomic force microscopy. *Colloids Surf. B Biointerfaces* **34**, 41–51 (2004).
155. Delorme, N. & Fery, A. Direct method to study membrane rigidity of small vesicles based on atomic force microscope force spectroscopy. *Phys. Rev. E Stat. Nonlin. Soft Matter Phys.* **74**, 030901 (2006).
156. Li, S., Eghiaian, F., Sieben, C., Herrmann, A. & Schaap, I. A. Bending and puncturing the influenza lipid envelope. *Biophys. J.* **100**, 637–645 (2011).
157. Vorselen, D. et al. Multilamellar nanovesicles show distinct mechanical properties depending on their degree of lamellarity. *Nanoscale* **10**, 5318–5324 (2018).
158. Engel, A. & Muller, D. J. Observing single biomolecules at work with the atomic force microscope. *Nat. Struct. Biol.* **7**, 715–718 (2000).
159. Muller, D. J., Buldt, G. & Engel, A. Force-induced conformational change of bacteriorhodopsin. *J. Mol. Biol.* **249**, 239–243 (1995).
160. Pfreundschuh, M., Hensen, U. & Muller, D. J. Quantitative imaging of the electrostatic field and potential generated by a transmembrane protein pore at subnanometer resolution. *Nano Lett.* **13**, 5585–5593 (2013).
161. Martinez-Martin, D., Herruzo, E. T., Dietz, C., Gomez-Herrero, J. & Garcia, R. Noninvasive protein structural flexibility mapping by bimodal dynamic force microscopy. *Phys. Rev. Lett.* **106**, 198101 (2011).
162. Wegmann, S. et al. Human Tau isoforms assemble into ribbon-like fibrils that display polymorphic structure and stability. *J. Biol. Chem.* **285**, 27302–27313 (2010).
163. Zhang, S. et al. Coexistence of ribbon and helical fibrils originating from hIAPP(20–29) revealed by quantitative nanomechanical atomic force microscopy. *Proc. Natl Acad. Sci. USA* **110**, 2798–2803 (2013).
164. de Pablo, P. J., Schaap, I. A. T., MacKintosh, F. C. & Schmidt, C. F. Deformation and collapse of microtubules on the nanometer scale. *Phys. Rev. Lett.* **91**, 098101 (2003).
165. Block, J. et al. Nonlinear loading-rate-dependent force response of individual vimentin intermediate filaments to applied strain. *Phys. Rev. Lett.* **118**, 048101 (2017).
166. Goodman, R. P. et al. Rapid chiral assembly of rigid DNA building blocks for molecular nanofabrication. *Science* **310**, 1661–1665 (2005).
167. Radmacher, M., Tillmann, R. W., Fritz, M. & Gaub, H. E. From molecules to cells: imaging soft samples with the atomic force microscope. *Science* **257**, 1900–1905 (1992).
168. Adamantidis, A. et al. Optogenetics: 10 years after Chr2 in neurons — views from the community. *Nat. Neurosci.* **18**, 1202–1212 (2015).
169. Seo, D. et al. A mechanogenetic toolkit for interrogating cell signaling in space and time. *Cell* **169**, 1357 (2017).
170. Dufrene, Y. F. et al. Five challenges to bringing single-molecule force spectroscopy into living cells. *Nat. Methods* **8**, 123–127 (2011).
171. Norregaard, K., Metzler, R., Ritter, C. M., Berg-Sorensen, K. & Oddershede, L. B. Manipulation and motion of organelles and single molecules in living cells. *Chem. Rev.* **117**, 4342–4375 (2017).
172. Derjaguin, B. V., Muller, V. M. & Toporov, Y. P. Effect of contact deformations on adhesion of particles. *J. Colloid Interface Sci.* **53**, 314–326 (1975).
173. Lomakina, E. B., Spillmann, C. M., King, M. R. & Waugh, R. E. Rheological analysis and measurement of neutrophil indentation. *Biophys. J.* **87**, 4246–4258 (2004).
174. Rosenbluth, M. J., Lam, W. A. & Fletcher, D. A. Force microscopy of nonadherent cells: a comparison of leukemia cell deformability. *Biophys. J.* **90**, 2994–3003 (2006).
175. de Sousa, J. S. et al. Analytical model of atomic-force-microscopy force curves in viscoelastic materials exhibiting power law relaxation. *J. Appl. Phys.* **121**, 034901 (2017).
176. Darling, E. M., Zauscher, S. & Guilak, F. Viscoelastic properties of zonal articular chondrocytes measured by atomic force microscopy. *Osteoarthritis Cartilage* **14**, 571–579 (2006).
177. Stifter, T., Weilandt, E., Marti, O. & Hild, S. Influence of the topography on adhesion measured by SFM. *Appl. Phys. A* **66**, S597–S605 (1998).
178. Rico, F. et al. Probing mechanical properties of living cells by atomic force microscopy with blunted pyramidal cantilever tips. *Phys. Rev. E* **72**, 021914 (2005).

Acknowledgements

The authors thank R. Newton for critically discussing the manuscript. M.K. acknowledges financial support from the Spanish Ministry of Economy and Competitiveness through the Ramon y Cajal programme (RYC-2015-17935), “Severo Ochoa” programme for the Centres of Excellence in R&D (SEV-2015-0522) from Fundació Privada Cellex, Generalitat de Catalunya, through the Centres de Recerca de Catalunya (CERCA) programme, and the European Research Council (ERC: MechanoSystems grant 715243). D.A. was supported by the ERC (NanoVirus grant 758224) and the National Fund for Scientific Research and Research Department of the Communauté française de Belgique (Concerted Research Action). B.M.G. was supported by a long-term European Molecular Biology Organization (EMBO) fellowship (ALTF 424–2016). W.H.R. was funded by the Nederlandse organisatie voor Wetenschappelijk Onderzoek (VIDI grant). H.E.G. acknowledges financial support from the CelluFuel ERC grant. C.G. was supported by the Swiss Nanoscience Institute (SNI), University of Basel. Y.F.D. was supported by the Université catholique de Louvain, ERC, under the European Union’s Horizon 2020 research and innovation programme (grant 693630), Walloon Excellence in Life Sciences and Biotechnology (WELBIO) (grant no. WELBIO-CR-2015A-05), National Fund for Scientific Research (FNRS and EOS grants) and Research Department of the Communauté française de Belgique (Concerted Research Action). D.J.M. was supported by the Swiss National Science Foundation (SNF; grant 310030B_160225), the National Centre of Competence in Research (NCCR) Molecular Systems Engineering and the Swiss Commission for Technology and Innovation (CTI, grant 28033.1).

Author contributions

All authors have read, discussed and contributed to the writing of the manuscript.

Competing interests

The authors declare no competing interests.

Publisher’s note

Springer Nature remains neutral with regard to jurisdictional claims in published maps and institutional affiliations.